Effects of pairing strength on the nuclear structure and double-β decay predictions within the mapped interacting boson model

K. Nomura[*]

Department of Physics, Hokkaido University, Sapporo 060-0810, Japan
and Nuclear Reaction Data Center, Hokkaido University, Sapporo 060-0810, Japan

The low-energy nuclear structure and two-neutrino double-β ($2\nu\beta\beta$) decay are studied within the interacting boson model (IBM) that is based on the nuclear energy density functional (EDF). The IBM Hamiltonian describing the initial and final even-even nuclei, and the interacting boson fermion-fermion Hamiltonian producing the intermediate states of the neighboring odd-odd nuclei are determined by the microscopic inputs provided by the self-consistent mean-field (SCMF) calculations employing a relativistic EDF and a separable pairing force. Sensitivities of the low-lying structure and $2\nu\beta\beta$-decay properties to the pairing strength are specifically analyzed. It is shown that the SCMF calculations with decreased and increased pairing strengths lead to quadrupole-quadrupole interaction strengths in the IBM that are, respectively, significantly enhanced and reduced in magnitude. When the increased pairing is adopted, in particular, the energy levels of the excited 0^+ states are lowered, and the predicted $2\nu\beta\beta$-decay nuclear matrix elements (NMEs) increase in magnitude systematically. The mapped IBM employing the increased pairing force generates effective NMEs and half-lives that are in a reasonable agreement with the experimental data for the $^{76}\text{Ge} \rightarrow {}^{76}\text{Se}$, $^{82}\text{Se} \rightarrow {}^{82}\text{Kr}$, and $^{100}\text{Mo} \rightarrow {}^{100}\text{Ru}$ decays in particular, whereas the calculation with the standard pairing strength is adequate to provide an overall good description of the effective NMEs in agreement with data.

I. INTRODUCTION

The double-β ($\beta\beta$) decay is a rare nuclear process by which the neutron N and proton Z numbers decrease (or increase) and increase (or decrease) by two, emitting two electrons (positrons) and some light particles such as neutrinos. Since this nuclear decay process, especially the one that does not emit neutrinos (neutrinoless $\beta\beta$ decay: $0\nu\beta\beta$) concerns several conservation laws required for the electroweak fundamental interactions in the standard model, and the nature and masses of neutrinos, a number of underground experiments aimed to detect the $\beta\beta$ decay have been running and proposed all over the world [1–9]. See also, e.g., Refs. [10–12] for a review on the related experimental investigations.

Theoretical studies on the $\beta\beta$ decay in the context of low-energy nuclear physics mainly consist in the calculations of the corresponding nuclear matrix elements (NMEs). The predicted $\beta\beta$ NMEs currently available are, however, largely at variance with different theoretical approaches by a factor of 2 to 3. Reducing the theoretical uncertainties arising in a given nuclear model is, therefore, a crucial step toward the consistent understanding of the $\beta\beta$ decay. Accurate computations of the NMEs would be, in turn, a stringent test for the model, as the nuclear wave functions used to compute the NMEs should be sensitive to the model's assumptions, parameters, etc. The two-neutrino $\beta\beta$ ($2\nu\beta\beta$) decay, in particular, is an allowed

decay, and a number of experimental data are available (see, e.g., [13–17]) to compare with theoretical calculations. For the calculations of the $2\nu\beta\beta$ decay, the so-called closure approximation, which is considered valid for the 0ν modes, is not a good approximation, but the intermediate states of the neighboring odd-odd nuclei should be explicitly taken into account. Theoretical predictions on the $2\nu\beta\beta$-decay NMEs that do not assume the closure approximation have been reported, such as in the quasiparticle random phase approximation (QRPA) [5,18,19], nuclear shell model (NSM) [20–25], and interacting boson model (IBM) [26].

Recently, a calculation of the two-neutrino $\beta\beta$ decay ($2\nu\beta\beta$) NMEs of a number of candidate nuclei was reported [27], employing the neutron-proton IBM (IBM-2) [28,29] that is based on the self-consistent mean-field (SCMF) calculation within the framework of the nuclear energy density functional (EDF) [30–34]. In that study, the IBM-2 Hamiltonians producing the low-lying states of the initial even-even nuclei including ^{48}Ca to ^{198}Pt, and those of the final ones including ^{48}Ti to ^{198}Hg, were completely determined so that the triaxial quadrupole potential energy surface (PES), which is obtained from the constrained relativistic Hartree-Bogoliubov (RHB) [32,33] SCMF calculation employing the density-dependent point-coupling (DD-PC1) [35] EDF and the separable pairing force of finite range [36], is mapped onto that of the boson system. The calculation for the $2\nu\beta\beta$-decay NMEs was made without the closure approximation, and the intermediate odd-odd nuclei were treated in terms of the particle-core coupling scheme within the neutron-proton interacting

---

[*]Contact author: nomura@sci.hokudai.ac.jp

boson-fermion-fermion model (IBFFM-2) [37,38], with the building blocks being also determined by the same SCMF calculation.

The mapped IBM-2 study of Ref. [27] has shown that the calculated $2\nu\beta\beta$-decay NMEs with mass-dependent quenching factors generally fell into the spectrum of various theoretical values available in the literature, and were more less consistent with the experimental systematic [13]. The amounts of the quenching were, however, shown to be also different among the decay processes. For instance, the NME for the ^{76}Ge $\rightarrow$ ^{76}Se decay was calculated to be substantially small to such an extent that does not require a quenching, whereas a too large NME was obtained for the ^{150}Nd $\rightarrow$ ^{150}Sm decay, for which a much larger quenching than the former, approximately by a factor of 5, was needed. The fact that the quenching of the NMEs was required, and that it was at variance with the decay processes indicated a need for further investigating possible uncertainties in the mapped IBM-2 descriptions. Indeed, dependencies of the $2\nu\beta\beta$-decay NMEs on several model assumptions and parameters within this framework were studied in Ref. [27], and it was suggested that a possible refinement of the model could be made, for instance, at the level of the SCMF calculations and/or the employed EDF, on which the IBM-2 and IBFFM-2 Hamiltonians and the $2\nu\beta\beta$-decay operators were built.

It is the aim of the present article to pursue further the last point, that is, to explore the sensitivities of the mapped IBM-2 predictions on the $2\nu\beta\beta$-decay NMEs, along with the properties of the low-lying states of the relevant even-even and odd-odd nuclei, to the underlying SCMF calculations. Among those controllable parameters in the SCMF model, in the present study the effects of the pairing strength in the RHB-SCMF calculations on the mapped IBM-2 predictions are specifically analyzed for those candidate nuclei, ^{48}Ca, ^{76}Ge, ^{82}Se, ^{96}Zr, ^{100}Mo, ^{116}Cd, ^{128}Te, ^{130}Te, ^{136}Xe, and ^{150}Nd, where experimental data are available.

In previous applications of the mapped IBM-2 to a number of nuclear structure phenomena, there has been a problem that the microscopically derived quadrupole-quadrupole boson interaction strength in the IBM-2 Hamiltonian, responsible for deformation, is considerably larger in magnitude than those used in the conventional IBM fits, and this leads to substantial deviations from the observed low-lying energy spectra, such as that of the excited 0^+ states, which are generally predicted to be too high as compared to the experimental data. On one hand, this has been handled on the IBM's side, that is, either by incorporating the effects of configuration mixing [39], i.e., the mixing between several configurations associated with particle-hole excitations that are different in boson numbers (see, e.g., Refs. [40–42]), or by introducing dynamical pairing degree of freedom as additional collective coordinate to the quadrupole deformations [43,44]. On the other hand, the discrepancy in the calculation of the excited 0^+ states has been, in many cases, attributed to the properties of the underlying SCMF calculations also, since any of the representative relativistic and nonrelativistic EDFs appears to produce PESs that are steep in both β and γ deformations, and exhibit a too pronounced energy minimum to be used as an input to the IBM.

Increasing the strength of the pairing correlations would soften the PES, as the stronger pairing generally favors a less deformed configuration, so that the quadrupole-quadrupole strength in the IBM-2 is expected to be reasonably reduced. The increased pairing strength in both the relativistic and nonrelativistic EDF frameworks has been shown to provide a better agreement with the experimental energy spectrum of the deformed nucleus ^{168}Er in the mapped IBM [45]. It was shown more recently that the reduction of the bosonic quadrupole-quadrupole interaction strength allows one to reproduce the measured log ft values for the single-β decays in the neutron-rich even-even Zr isotopes [46].

The paper is organized as follows. Section II describes the theoretical procedure. The results of the nuclear structure calculations for each even-even and odd-odd nucleus, excitation spectra, and electromagnetic transition properties are presented in Sec. III. Section IV presents results of the calculated $2\nu\beta\beta$-decay NMEs and half-lives resulting from the different pairing strengths in comparison to the experimental data. A summary and concluding remarks are given in Sec. V.

II. THEORETICAL FRAMEWORK

A. Self-consistent mean-field calculations

To obtain the microscopic inputs to the IBM-2 and IBFFM-2 Hamiltonians, the triaxial quadrupole constrained SCMF calculations are carried out employing the RHB method [32,33] with the particle-hole channel given by the DD-PC1 interaction. The particle-particle part is modeled by the separable pairing force of finite range [36], with the pairing matrix element defined in the coordinate space

$$V(\mathbf{r}_1, \mathbf{r}_2, \mathbf{r}'_1, \mathbf{r}'_2) = -V\delta(\mathbf{R} - \mathbf{R}')P(\mathbf{r})P(\mathbf{r}')\tfrac{1}{2}(1 - P^\sigma), \quad (1)$$

where $\mathbf{R} = (\mathbf{r}_1 + \mathbf{r}_2)/2$ and $\mathbf{r} = \mathbf{r}_2 - \mathbf{r}_2$ are the center-of-mass and relative coordinates, respectively, and the factor $P(\mathbf{r})$ a Gaussian function

$$P(\mathbf{r}) = \frac{1}{(4\pi a^2)^{3/2}}e^{-\mathbf{r}^2/4a^2}. \quad (2)$$

The strength $V = 728$ MeV fm^3 and the parameter $a = 0.644$ fm are taken to be the same for protons and neutrons, and these values were determined in [36] so that the $^1S_0$ pairing gap of infinite nuclear matter resulting from the Hartree-Fock-Bogoliubov (HFB) model calculation using the Gogny-D1S EDF [47] should be reproduced. In the present study, in addition to the default value $V = 728$ MeV fm^3 two other values are employed for the RHB-SCMF calculations: 655 and 837 MeV fm^3, which correspond to the decrease and increase of the original value V by 10% and 15%, respectively. The other parameter, a, is here kept constant for the sake of simplicity.

The particular choices of the pairing strength, i.e., scaling it with factors 0.9 and 1.15, are here considered as two illustrative cases in which quantitative changes in various calculated results on the low-lying states and $2\nu\beta\beta$ decay are clearly observed. Use of the above two scaling factors is also inspired by a global systematic study of the separable pairing strength within the relativistic EDF, that was reported in Ref. [48]. In that study, global fits of the pairing interaction strength to the

empirical odd-even mass staggering over the entire mass table suggest that the strength does depend on nucleon numbers, and for majority of the studied nuclei the modified pairing strengths with the scaling factor f, being typically within the range $0.9 \lesssim f \lesssim 1.2$, were considered for medium-mass and heavy regions. In addition, the earlier mapped IBM study on the ^{168}Er energy spectrum [45] reported a generally more reasonable description of the low-lying non-yrast levels including that of the excited 0_2^+ state with the increased pairing by 15% than with the default strength.

A set of the RHB-SCMF calculations are performed for each even-even nucleus with constraints on the mass quadrupole moments that are associated with the triaxial quadrupole deformations β and γ in the geometrical model [49]. The RHB-SCMF calculations yield the potential energy surface (PES), that is, total mean-field energy defined as a function of the β and γ deformations, and then it is used as the input to construct the IBM-2 Hamiltonian. The RHB-SCMF calculations further provide single-particle energies, and occupation probabilities at spherical configuration for the neighboring odd-odd nuclei. These quantities are to be used to construct the IBFFM-2 Hamiltonian, and are obtained from the standard RHB calculations without blocking, with constraints to zero deformation and with the particle number constrained to odd numbers (see Refs. [50,51] for details).

B. IBM-2 Hamiltonian

In order to calculate low-lying states and transition properties starting from the SCMF calculations, one should go beyond the mean-field approximation by restoring symmetries and including quantum fluctuations around the mean-field solution [30,31,33,34]. These so-called beyond-mean-field effects are here taken into account by mapping the SCMF results onto the IBM-2. The IBM-2 comprises the neutron s_ν and proton s_π monopole bosons, and neutron d_ν and proton d_π quadrupole bosons. The s_ν (s_π) and d_ν (d_π) bosons are connected to the collective monopole S_ν (S_π) and quadrupole D_ν (D_π) pairs of valence neutrons (protons) with spin and parity values $J = 0^+$ and $J = 2^+$, respectively [29].

The IBM-2 Hamiltonian employed in this study takes the form

$$\hat{H}_B = \epsilon_d\big(\hat{n}_{d_\nu} + \hat{n}_{d_\pi}\big) + \kappa \hat{Q}_\nu \cdot \hat{Q}_\pi + \kappa' \hat{L} \cdot \hat{L}. \tag{3}$$

$\hat{n}_{d_\rho} = d_\rho^\dagger \cdot \tilde{d}_\rho$ ($\rho = \nu, \pi$) is the d-boson number operator, with ϵ_d the single d-boson energy relative to the s-boson one, and $\tilde{d}_{\rho\mu} = (-1)^\mu d_{\rho-\mu}$. The second term is the quadrupole-quadrupole interaction between neutron and proton bosons, with $\hat{Q}_\rho = d_\rho^\dagger s_\rho + s_\rho^\dagger \tilde{d}_\rho + \chi_\rho(d_\rho^\dagger \times \tilde{d}_\rho)^{(2)}$ being the quadrupole operator in the boson system. The last term in Eq. (3) is a rotational term with $\hat{L} = \sqrt{10} \sum_\rho (d_\rho^\dagger \times \tilde{d}_\rho)^{(1)}$ being the bosonic angular momentum operator.

Since there appears no interaction between unlike-bosons for those nuclei corresponding either to $N_\pi = 0$ or $N_\nu = 0$, the following Hamiltonian is considered:

$$\hat{H}_B = \epsilon_{d\rho}\hat{n}_{d\rho} + \kappa_\rho \hat{Q}_\rho \cdot \hat{Q}_\rho, \tag{4}$$

which is nothing but the Hamiltonian in the IBM-1, where no distinction is made between neutron and proton bosons. The

IBM-1-like Hamiltonian (4) is here employed specifically for ^{48}Ca, ^{116}Sn, and ^{136}Xe, having $N_\pi = 0$, $N_\pi = 0$, and $N_\nu = 0$, respectively.

The strength parameters for the Hamiltonian (3), or (4), are determined by using the SCMF-to-IBM mapping procedure [52,53], so that the following approximate equality is satisfied in the vicinity of the global mean-field minimum:

$$E_{\text{SCMF}}(\beta, \gamma) \approx E_{\text{IBM}}(\beta, \gamma). \tag{5}$$

Here $E_{\text{SCMF}}(\beta, \gamma)$ represents the SCMF PES, and $E_{\text{IBM}}(\beta, \gamma)$ on the right-hand side the corresponding PES in the boson system, which is given as the energy expectation value $\langle\Phi|\hat{H}_B|\Phi\rangle / \langle\Phi|\Phi\rangle$, with the wave function $|\Phi\rangle$ being a boson coherent state [54,55] that is defined as

$$|\Phi\rangle = \prod_{\rho=\nu,\pi} \left[s_\rho^\dagger + \sum_{\mu=-2}^{+2} \alpha_{\rho\mu} d_{\rho\mu}^\dagger \right]^{N_\rho} |0\rangle, \tag{6}$$

up to the normalization factor. The amplitudes $\alpha_{\rho\mu}$ are given as $\alpha_{\rho 0} = \beta_\rho \cos\gamma_\rho$, $\alpha_{\rho\pm1} = 0$, and $\alpha_{\rho\pm2} = \beta_\rho \sin\gamma_\rho/\sqrt{2}$, where β_ρ and γ_ρ are boson analogs of the deformation variables. $|0\rangle$ represents the boson vacuum, i.e., the inert core. N_ν (N_π) is the number of neutron (proton) bosons, and is counted as half the number of valence neutron (proton) particles/holes with respect to the nearest doubly magic nucleus [28,29]. Only, for the ^{48}Ca and ^{48}Ti nuclei, the inert core is taken to be ^{40}Ca, in order to have the number of bosons be enough to produce boson-boson interactions. Furthermore, both the neutron and proton β_ρ and γ_ρ deformations are assumed to be equal to each other, $\beta_\nu = \beta_\pi$ and $\gamma_\nu = \gamma_\pi$. As in Ref. [27] it is also assumed that the β_ρ deformation is proportional to the geometrical one, $\beta_\nu = \beta_\pi \propto \beta$, while the γ_ρ is identical to the geometrical counterpart, $\gamma_\nu = \gamma_\pi \equiv \gamma$ [52,55].

The parameter κ' for the third term of Eq. (3), $\hat{L} \cdot \hat{L}$, is determined [56] separately from the other parameters, so that the cranking moment of inertia calculated in the intrinsic frame of the boson system [57] at the global minimum is equal to the corresponding Inglis-Belyaev [58,59] moment of inertia obtained from the RHB-SCMF calculation. This term is, however, neglected for most of the studied even-even nuclei, since it turns out to have only minor effects on the low-lying energy levels, except for a few nuclei with specific choices of the pairing strength. Details are given in Sec. III A 2.

C. IBFFM-2 Hamiltonian

The extension to the IBFFM-2 is made by introducing unpaired nucleon degrees of freedom and their couplings to the even-even IBM-2 space. The IBFFM-2 Hamiltonian is written as

$$\hat{H} = \hat{H}_B + \hat{H}_F^\nu + \hat{H}_F^\pi + \hat{V}_{BF}^\nu + \hat{V}_{BF}^\pi + \hat{V}_{\nu\pi}, \tag{7}$$

The first term $\hat{H}_B$ is the IBM-2 Hamiltonian (3) [or (4)]. The second and third terms represent the single-nucleon Hamiltonians of the form

$$\hat{H}_F^\rho = -\sum_{j_\rho} \epsilon_{j_\rho} \sqrt{2j_\rho + 1}\big(a_{j_\rho}^\dagger \times \tilde{a}_{j_\rho}\big)^{(0)} \equiv \sum_{j_\rho} \epsilon_{j_\rho}\hat{n}_{j_\rho}, \tag{8}$$

where ϵ_{j_ρ} stands for the single-particle energy of the odd neutron ($\rho = \nu$) or proton ($\rho = \pi$) orbital j_ρ. $a_{j_\rho}^{(\dagger)}$ represents a particle annihilation (or creation) operator, with $\tilde{a}_{j_\rho}$ defined by $\tilde{a}_{j_\rho m_\rho} = (-1)^{j_\rho - m_\rho} a_{j_\rho - m_\rho}$. The operator $\hat{n}_{j_\rho}$ stands for the number operator for the unpaired particle. Within the present formalism, the single-particle energy ϵ_{j_ρ} in Eq. (8) is replaced with the quasiparticle energy $\tilde{\epsilon}_{j_\rho}$.

The fourth (fifth) term of Eq. (7) stands for the interaction between the odd neutron (proton) and the IBM-2 core, and has a specific form [38]

$$\hat{V}_{\text{BF}}^\rho = \Gamma_\rho \hat{V}_{\text{dyn}}^\rho + \Lambda_\rho \hat{V}_{\text{exc}}^\rho + A_\rho \hat{V}_{\text{mon}}^\rho, \qquad (9)$$

where the first, second, and third terms are dynamical quadrupole, exchange, and monopole interactions, respectively. Expressions for the terms in Eq. (9) are given in the generalized seniority scheme as [38,60]

$$\hat{V}_{\text{dyn}}^\rho = \sum_{j_\rho j_\rho'} \gamma_{j_\rho j_\rho'} \left(a_{j_\rho}^\dagger \times \tilde{a}_{j_\rho'} \right)^{(2)} \cdot \hat{Q}_{\rho'}, \qquad (10)$$

$$\hat{V}_{\text{exc}}^\rho = -(s_{\rho'}^\dagger \times \tilde{d}_{\rho'})^{(2)} \cdot \sum_{j_\rho j_\rho' j_\rho''} \sqrt{\frac{10}{N_\rho (2j_\rho + 1)}} \beta_{j_\rho j_\rho'} \beta_{j_\rho'' j_\rho} :$$
$$\times \left[\left(d_\rho^\dagger \times \tilde{a}_{j_\rho''} \right)^{(j_\rho)} \times \left(a_{j_\rho'}^\dagger \times \tilde{s}_\rho \right)^{(j_\rho')} \right]^{(2)} : +(\text{H.c.}), \qquad (11)$$

$$\hat{V}_{\text{mon}}^\rho = \hat{n}_{d_\rho} \hat{n}_{j_\rho}, \qquad (12)$$

Here the factors $\gamma_{j_\rho j_\rho'} = (u_{j_\rho} u_{j_\rho'} - v_{j_\rho} v_{j_\rho'}) Q_{j_\rho j_\rho'}$ and $\beta_{j_\rho j_\rho'} = (u_{j_\rho} v_{j_\rho'} + v_{j_\rho} u_{j_\rho'}) Q_{j_\rho j_\rho'}$, with $Q_{j_\rho j_\rho'} = \langle \ell_\rho \frac{1}{2} j_\rho \| Y^{(2)} \| \ell_\rho' \frac{1}{2} j_\rho' \rangle$ the matrix element of the fermion quadrupole operator in the single-particle basis. $\hat{Q}_{\rho'}$ in (10) is the same boson quadrupole operator as in the boson Hamiltonian (3). The notation : $(\cdots)$: in (11) means normal ordering.

The last term of Eq. (7) corresponds to the odd neutron-proton interaction that is given as

$$\hat{V}_{\nu\pi} = 4\pi (v_d + v_{\text{ssd}} \boldsymbol{\sigma}_\nu \cdot \boldsymbol{\sigma}_\pi) \delta(\boldsymbol{r}) \delta(r_\nu - r_0) \delta(r_\pi - r_0)$$
$$- \frac{1}{\sqrt{3}} v_{\text{ss}} \boldsymbol{\sigma}_\nu \cdot \boldsymbol{\sigma}_\pi + v_t \left[\frac{3(\boldsymbol{\sigma}_\nu \cdot \boldsymbol{r})(\boldsymbol{\sigma}_\pi \cdot \boldsymbol{r})}{r^2} - \boldsymbol{\sigma}_\nu \cdot \boldsymbol{\sigma}_\pi \right]. \qquad (13)$$

The first term consists of the δ, and spin-spin δ interactions, and the second, and third terms represent the spin-spin and tensor interactions, respectively. v_d, v_{ssd}, v_{ss}, and v_t are strength parameters. Note that $\boldsymbol{r} = \boldsymbol{r}_\nu - \boldsymbol{r}_\pi$ is the relative coordinate of the neutron and proton, and $r_0 = 1.2 A^{1/3}$ fm.

The strength parameters for the IBFFM-2 Hamiltonian (7) are obtained by using the procedure developed in Refs. [50,61]: (i) The quasiparticle energies $\tilde{\epsilon}_{j_\rho}$, occupation v_{j_ρ}, and unoccupation u_{j_ρ} amplitudes provided by the RHB-SCMF calculations are input to $\hat{H}_F^\rho$ (8) and $\hat{V}_{\text{BF}}^\rho$ (9); (ii) the coupling constants Γ_ρ, Λ_ρ, and A_ρ are fit to reproduce a few low-lying levels of each of the neighboring odd-N and odd-Z nuclei, separately for positive- and negative-parity states; (iii) the parameters for $\hat{V}_{\nu\pi}$ (13) are determined so as to reproduce the ground-state spin and a few energy levels of each odd-odd nucleus. The employed parameters for the IBFFM-2 Hamiltonian are given in Tables VI, VII, and VIII in the Appendix. Single-particle spaces taken for the odd nucleons are

given in Tables VI and VII. The even-even boson core nuclei and neighboring odd-N and odd-Z nuclei are summarized in Table I of Ref. [27].

D. $2\nu\beta\beta$ decay operators

The $2\nu\beta\beta$-decay NME requires to calculate the Gamow-Teller (GT) and Fermi (F) transitions for the single-β decay from the initial even-even to intermediate odd-odd, and that from the intermediate odd-odd, to final even-even nuclei. The corresponding GT and F operators take the forms

$$\hat{T}^{\text{GT}} = \sum_{j_\nu j_\pi} \eta_{j_\nu j_\pi}^{\text{GT}} \left(\hat{P}_{j_\nu} \times \hat{P}_{j_\pi} \right)^{(1)}, \qquad (14)$$

$$\hat{T}^{\text{F}} = \sum_{j_\nu j_\pi} \eta_{j_\nu j_\pi}^{\text{F}} \left(\hat{P}_{j_\nu} \times \hat{P}_{j_\pi} \right)^{(0)}, \qquad (15)$$

where the coefficients $\eta_{j_\nu j_\pi}^{\text{GT}}$ and $\eta_{j_\nu j_\pi}^{\text{F}}$ are, to the lowest order,

$$\eta_{j_\nu j_\pi}^{\text{GT}} = -\frac{1}{\sqrt{3}} \left\langle \ell_\nu \frac{1}{2}; j_\nu \left\| \boldsymbol{\sigma} \right\| \ell_\pi \frac{1}{2}; j_\pi \right\rangle \delta_{\ell_\nu \ell_\pi}, \qquad (16)$$

$$\eta_{j_\nu j_\pi}^{\text{F}} = -\sqrt{2j_\nu + 1} \delta_{j_\nu j_\pi}. \qquad (17)$$

$\hat{P}_{j_\rho}$ is here given by one of the one-particle creation operators

$$A_{j_\rho m_\rho}^\dagger = \zeta_{j_\rho} a_{j_\rho m_\rho}^\dagger + \sum_{j_\rho'} \zeta_{j_\rho j_\rho'} s_\rho^\dagger \left(\tilde{d}_\rho \times a_{j_\rho'}^\dagger \right)_{m_\rho}^{(j_\rho)}, \qquad (18a)$$

$$B_{j_\rho m_\rho}^\dagger = \theta_{j_\rho} s_\rho^\dagger \tilde{a}_{j_\rho m_\rho} + \sum_{j_\rho'} \theta_{j_\rho j_\rho'} \left(d_\rho^\dagger \times \tilde{a}_{j_\rho'} \right)_{m_\rho}^{(j_\rho)} \qquad (18b)$$

and annihilation operators

$$\tilde{A}_{j_\rho m_\rho} = (-1)^{j_\rho - m_\rho} A_{j_\rho - m_\rho}, \qquad (18c)$$

$$\tilde{B}_{j_\rho m_\rho} = (-1)^{j_\rho - m_\rho} B_{j_\rho - m_\rho}. \qquad (18d)$$

The operators in Eqs. (18a) and (18c) conserve the boson number, whereas those in Eqs. (18b) and (18d) do not. The GT (14) and Fermi (15) operators are formed as a pair of the above operators, depending on the particle or hole nature of bosons in the even-even IBM-2 core. Coefficients ζ_j, $\zeta_{jj'}$, θ_j, and $\theta_{jj'}$ are dependent on the v_{j_ρ} and u_{j_ρ} amplitudes, for which the same values as those used in the IBFFM-2 calculations for the odd-odd nuclei are employed. The expressions for these coefficients are found, e.g., in Appendix D of Ref. [27]. A more detailed description of the derivation of the one-particle transfer operator within the generalized seniority scheme is found in Refs. [38,62,63].

The GT and F matrix elements that enter the $2\nu\beta\beta$ NME are calculated via the formulas

$$M_{2\nu}^{\text{GT}} = \sum_N \frac{\langle 0_F^+ \| \hat{T}^{\text{GT}} \| 1_N^+ \rangle \langle 1_N^+ \| \hat{T}^{\text{GT}} \| 0_{1,I}^+ \rangle}{E_N - E_I + \frac{1}{2}(Q_{\beta\beta} + 2m_e c^2)}, \qquad (19)$$

$$M_{2\nu}^{\text{F}} = \sum_N \frac{\langle 0_F^+ \| \hat{T}^{\text{F}} \| 0_N^+ \rangle \langle 0_N^+ \| \hat{T}^{\text{F}} \| 0_{1,I}^+ \rangle}{E_N - E_I + \frac{1}{2}(Q_{\beta\beta} + 2m_e c^2)}, \qquad (20)$$

respectively. In the denominators E_I (E_N) stands for the energy of the initial (intermediate) state, $Q_{\beta\beta}$ is the Q value for the $2\nu\beta\beta$ decay, and m_e is the electron mass, i.e., $m_e = 0.511$ MeV/c^2. The sums in Eqs. (19) and (20) are taken

TABLE I. Calculated electric quadrupole $Q(I)$ (in eb) and magnetic dipole $\mu(I)$ (in μ_N) moments, and the $B(M1)$ transition strengths (in W.u.) of the intermediate odd-odd nuclei, obtained from the RHB-SCMF mapped IBFFM-2 with the reduced ($0.9V$), default (V), and increased ($1.15V$) pairing strengths. The experimental values are taken from Refs. [64,66].

Nucleus	Property	IBFFM-2			Experiment
		$0.9V$	V	$1.15V$	
^{48}Sc	$\mu(6_1^+)$	3.100	3.098	3.091	$+3.737 \pm 0.012$
^{76}As	$\mu(1_1^+)$	-0.095	0.388	2.235	$+0.559 \pm 0.005$
^{96}Nb	$\mu(6_1^+)$	-0.479	4.547	-0.874	4.976 ± 0.004
	$B(M1; 4_1^+ \rightarrow 5_1^+)$	0.0039	1.2298	0.0263	>0.021
	$B(M1; 2_1^+ \rightarrow 3_1^+)$	0.0030	0.2426	0.0025	>0.00017
^{116}In	$\mu(1_1^+)$	2.958	2.478	2.996	$+2.7876 \pm 0.0006$
	$Q(1_1^+)$	0.126	0.213	0.110	0.11
	$\mu(5_1^+)$	0.870	0.177	0.505	4.435 ± 0.015
	$Q(5_1^+)$	-0.764	-0.813	-0.747	$+0.802 \pm 0.012$
	$B(M1; 4_1^+ \rightarrow 5_1^+)$	0.0002	0.0072	0.0054	>0.18
	$B(M1; 2_1^+ \rightarrow 1_1^+)$	0.1236	0.2249	0.0549	>0.016
	$B(M1; 4_2^+/5_2^+ \rightarrow 4_1^+)$	0.0010/0.1709	0.0621/0.0060	0.0616/0.0687	0.00013 ± 0.00006
	$B(M1; 4_2^+/5_2^+ \rightarrow 5_1^+)$	0.0013/0.0085	0.0002/0.0275	0.0148/0.0044	0.00013 ± 0.00006
	$B(M1; 3_1^+ \rightarrow 4_1^+)$	0.0014	0.0090	0.0005	>0.0080
	$B(M1; 3_1^+ \rightarrow 2_1^+)$	0.0232	0.1079	0.0505	>0.0066
^{128}I	$B(M1; 3_2^+ \rightarrow 3_1^+)$	0.0002	0.0068	0.0034	>0.0017
	$B(M1; 3_2^+ \rightarrow 2_1^+)$	0.0088	0.0011	0.0005	>0.011
	$B(M1; 1_2^+/2_2^+ \rightarrow 2_1^+)$	0.6268/0.0090	0.0022/0.0223	0.0170/0.0166	>0.0026
	$B(M1; 1_2^+/2_2^+ \rightarrow 1_1^+)$	0.1847/0.0085	0.0004/0.0006	0.0002/0.0044	>0.0046
	$B(M1; 3_3^+ \rightarrow 2_2^+)$	0.0036	0.0041	0.0092	>0.0095
	$B(M1; 3_3^+ \rightarrow 3_1^+)$	0.0000	0.0087	0.0002	>0.00011
	$B(M1; 3_3^+ \rightarrow 2_1^+)$	0.0000	0.0021	0.0185	>0.00051
	$B(M1; 4_2^+ \rightarrow 3_1^+)$	0.0267	0.0542	0.0105	>0.0027
	$B(M1; 4_2^+ \rightarrow 3_2^+)$	0.4234	0.0733	0.1520	>0.0019
	$B(M1; 4_2^+ \rightarrow 4_1^+)$	0.0048	0.0045	0.0855	>0.00050
^{130}I	$\mu(5_1^+)$	2.606	3.900	2.845	3.349 ± 0.007
^{136}Cs	$\mu(5_1^+)$	2.381	3.570	2.379	$+3.711 \pm 0.005$
	$Q(5_1^+)$	0.196	0.267	0.191	$+0.225 \pm 0.010$

over all the intermediate states 1_N^+ and 0_N^+ obtained from the IBFFM-2 Hamiltonian below the excitation energy of 30 MeV. For the $Q_{\beta\beta}$ value, experimental data available at NNDC database [64] are adopted. Using $M_{2\nu}^{\mathrm{GT}}$ (19) and $M_{2\nu}^{\mathrm{F}}$ (20) transition matrix elements, the $2\nu\beta\beta$-decay NME is obtained through

$$M_{2\nu} = g_A^2 m_e c^2 \left[M_{2\nu}^{\mathrm{GT}} - \left(\frac{g_V}{g_A} \right)^2 M_{2\nu}^{\mathrm{F}} \right], \qquad (21)$$

with $g_V = 1$ and $g_A = 1.269$ the vector and axial vector coupling constants, respectively. The corresponding half-life, denoted $\tau_{1/2}^{(2\nu)}$, can be readily calculated by [4]

$$\left[\tau_{1/2}^{(2\nu)} \right]^{-1} = G_{2\nu} |M_{2\nu}|^2, \qquad (22)$$

where $G_{2\nu}$ is the phase-space factor in year^{-1} for the $0^+ \rightarrow 0^+$ $2\nu\beta\beta$ decay. The $G_{2\nu}$ values calculated in Ref. [65] are used.

III. LOW-ENERGY NUCLEAR STRUCTURES

A. Even-even nuclei

1. Potential energy surfaces

Figures 1 and 2 display the PESs in terms of the quadrupole triaxial (β, γ) deformations for the even-even initial and final nuclei, obtained from the constrained RHB-SCMF calculations employing the DD-PC1 EDF, combined with the reduced ($0.9V$), default (V), and increased ($1.15V$) strengths of the separable pairing force (1). The PESs with the default pairing strength are taken from Ref. [27] without any change, and their properties were discussed there. A general effect of reducing the pairing strength is that the potential becomes steeper in both β and γ deformations, and in some cases the global minimum occurs at a larger β deformation. If one increases the pairing strength with respect to the default one, on the other hand, the PES generally looks even softer in β and γ deformations, and the location of the global minimum shifts in the direction to the origin, hence disfavoring the strong deformation.

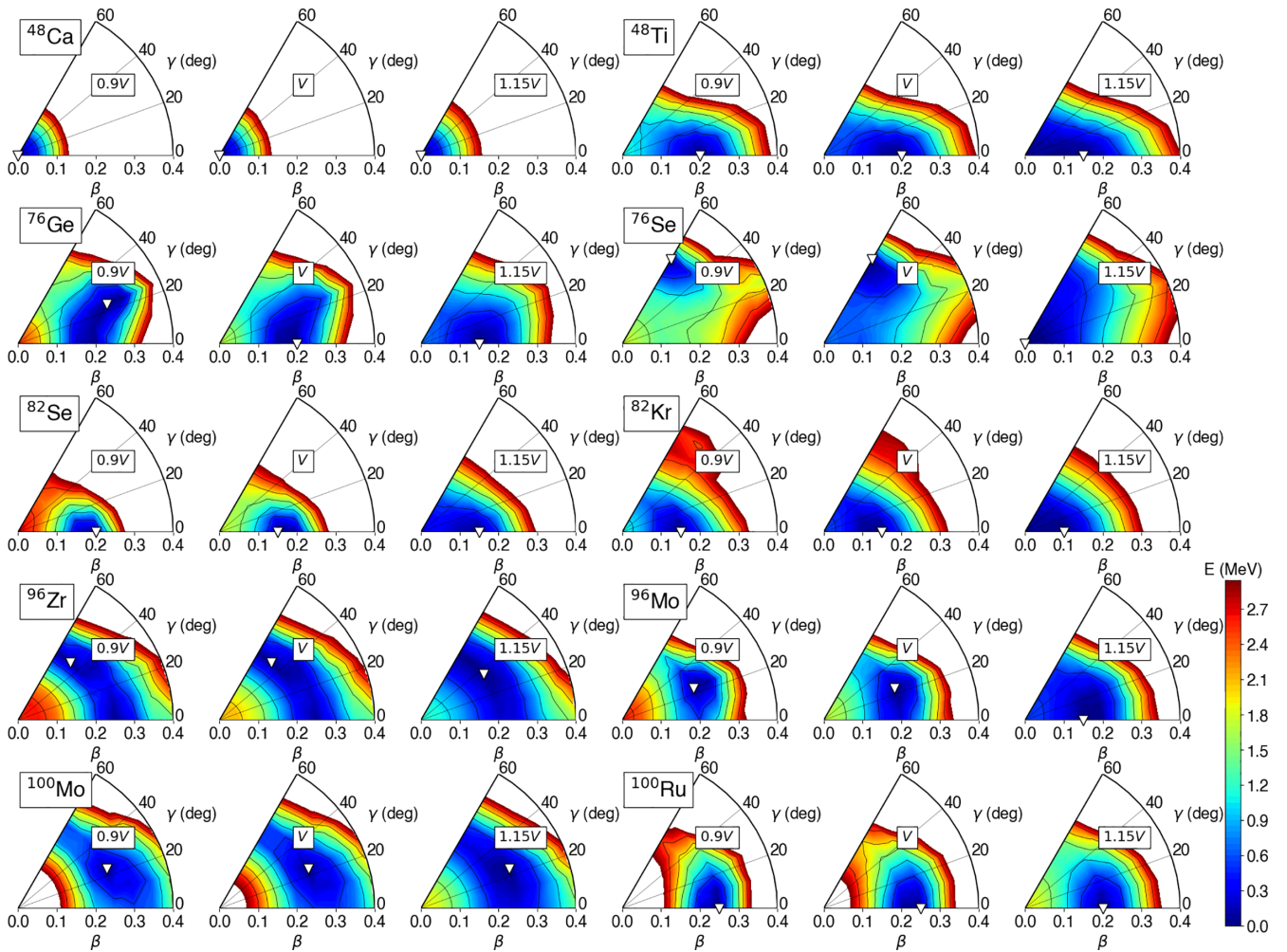FIG. 1. Triaxial quadrupole (β, γ) potential energy surfaces for the even-even nuclei from ^{48}Ca to ^{100}Ru obtained from the constrained SCMF calculations within the RHB method using the DD-PC1 EDF and the separable pairing force with strengths $0.9V = 655$ MeV fm^3 (first and fourth columns), $V = 728$ MeV fm^3 (second and fifth columns), and $1.15V = 837$ MeV fm^3 (third and sixth columns). The energy difference between neighboring contours is 0.3 MeV, and the global minimum is indicated by the open triangle.

Figure 3 shows the energies (a) E_{def}, defined as the difference between the mean-field energies at the origin and at the global minimum, and (b) E_γ, defined as the difference in energy between the global minimum and saddle point along axial deformation, i.e., the $\gamma = 0°$ and $60°$ axes. The former quantity represents an energy gained by the deformation, while the latter can be used as a measure of the γ softness. It is seen from Fig. 3 that the quantity E_{def} is reduced (increased) by a few MeV when the increased $1.15V$ (reduced $0.9V$) pairing strength is used. The increased pairing strength generally leads to a lower E_γ energy, implying that the PES becomes softer in γ deformation.

The corresponding IBM-2 PES in the case of the default pairing strength V were presented in Ref. [27]. It was shown [27] that the basic features of the SCMF PESs in the neighborhood of the global minimum are reproduced by the IBM-2. Discrepancies between the SCMF and IBM-2 PESs in their topology were shown to arise such that the latter is in most cases flatter in the region of large β deformations, and that triaxial minima found in the SCMF PESs for ^{96}Zr, ^{96}Mo,

^{100}Mo, ^{128}Te, and ^{130}Xe cannot be reproduced in the IBM-2 surfaces. These discrepancies can be attributed to the limited degrees of freedom and form of the Hamiltonian in the IBM-2. Similar observations hold for the mapped IBM-2 PESs both with the reduced and increased pairing strengths.

2. Derived IBM-2 parameters

Figure 4 shows the derived parameters for the IBM-2 Hamiltonian (3) for the even-even nuclei. What is worth noticing are the facts that the derived single-d boson energy ϵ_d [Figs. 4(a) and 4(b)] is basically larger when a larger pairing strength is considered, and that the quadrupole-quadrupole interaction strength κ derived in the case of a stronger pairing force is systematically reduced in magnitude, most notably, by approximately a factor of 4 for ^{136}Ba [Figs. 4(c) and 4(c)].

In addition, the ratio of these parameters, $|\kappa|/\epsilon_d$, is systematically lowered for the increased pairing strength, representative cases being ^{76}Ge, ^{128}Te, ^{100}Ru, ^{128}Xe, and ^{130}Xe. In the case of ^{76}Ge, for instance, the ratios corresponding
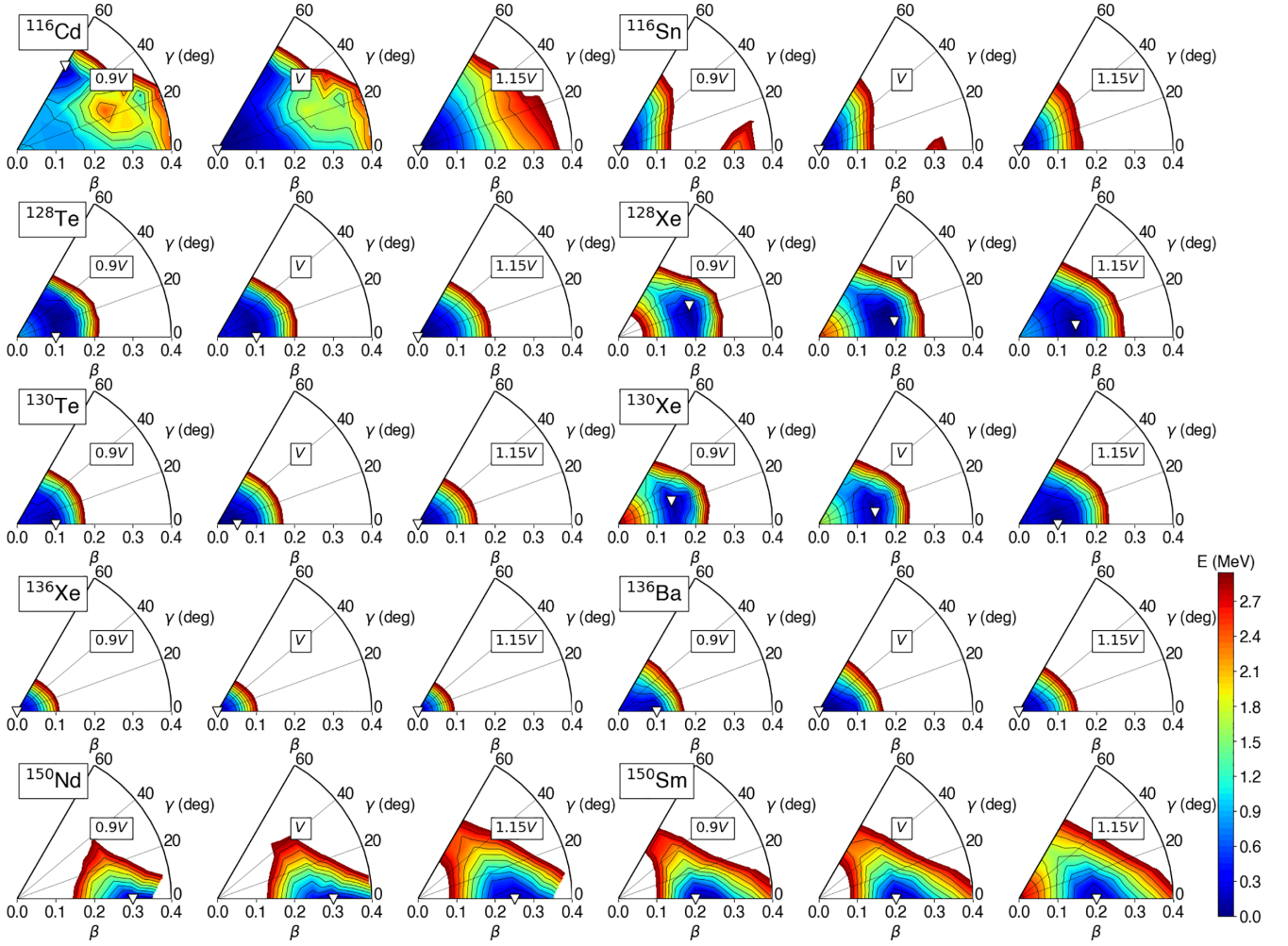
FIG. 2. Same as Fig. 1, but for the even-even nuclei from ^{116}Cd to ^{150}Sm.

to 0.9V, V, and 1.15V pairing strengths are 1.1, 0.88, and 0.47, respectively. Since the $\hat{n}_d$ term favors a spherical shape and the $\hat{Q}_\nu \cdot \hat{Q}_\pi$ term gives rise to deformation, the ratio of their strength parameters $|\kappa|/\epsilon_d$ provides an implication for the degree of deformation and collectivity. The reduction of the ratio with the increased pairing strength is reasonable, as the pairing correlations generally prefer a less deformed shape, and indeed the SCMF PES tends to be softer with enhanced pairing strength (cf. Fig. 3).

From Figs. 4(e) to 4(h) the derived parameters χ_ν and χ_π do not depend much on the pairing strengths. A few exceptions are perhaps the χ_ν values for ^{116}Cd, and ^{76}Se, for which the values corresponding to the pairing strengths of 0.9V and 1.15V are quite large and small, respectively. This reflects the fact that the SCMF PESs for these nuclei exhibit a more pronounced potential valley on the oblate side with the reduced pairing strength (see Figs. 1 and 2).

As noted, in the present IBM-2 calculations the $\hat{L} \cdot \hat{L}$ term is considered only for ^{150}Nd, ^{150}Sm, ^{96}Zr, and ^{76}Se when particular pairing strengths are considered. For these nuclei, this term has certain influences on the energy spectra, and the corresponding strength parameter κ' are also

appreciable: for ^{150}Nd the values $\kappa' = -0.0082$ MeV (with V) and -0.024 MeV (with 0.9V); for ^{150}Sm $\kappa' = 0.0095$ MeV (with V) and 0.022 MeV (with 1.15V); for ^{96}Zr $\kappa' = 0.021$ MeV (with V) and 0.063 MeV (with 1.15V); and for ^{76}Se $\kappa' = 0.021$ MeV (with V) are employed.

The parameters for the like-boson interactions in Eq. (4) specifically considered for the semimagic nuclei are as follows. $\epsilon_{d\nu} = 1.5$ MeV and $\kappa_\nu = -0.057$ MeV (^{48}Ca, and ^{116}Sn); $\chi_\nu = 0.8$ (^{116}Sn) and 0 (^{48}Ca); and $\epsilon_{d\pi} = 1.5$ MeV, $\kappa_\pi = -0.057$ MeV, and $\chi_\pi = -0.8$ for ^{138}Xe. These values are taken to be the same between the IBM-2 calculations based on the different pairing strengths.

Concerning the $2\nu\beta\beta$ decays of ^{48}Ca, ^{116}Cd, and ^{150}Nd, the boson core nuclei for the odd-odd intermediate nuclei ^{48}Sc, ^{116}In, and ^{150}Pm are taken to be ^{46}Ca, ^{118}Sn, and ^{148}Nd, respectively, which are different from either of the initial and final nuclei. The IBM-2 parameters used for these boson core nuclei are shown in Table IX of Ref. [27] in the case of the default pairing strength, and the same parameters are here employed. As for the ^{46}Ca and ^{118}Sn nuclei, the same IBM-2 parameters are used for the calculations with the modified pairing strengths 0.9V and 1.15V. Regarding ^{148}Nd, however,
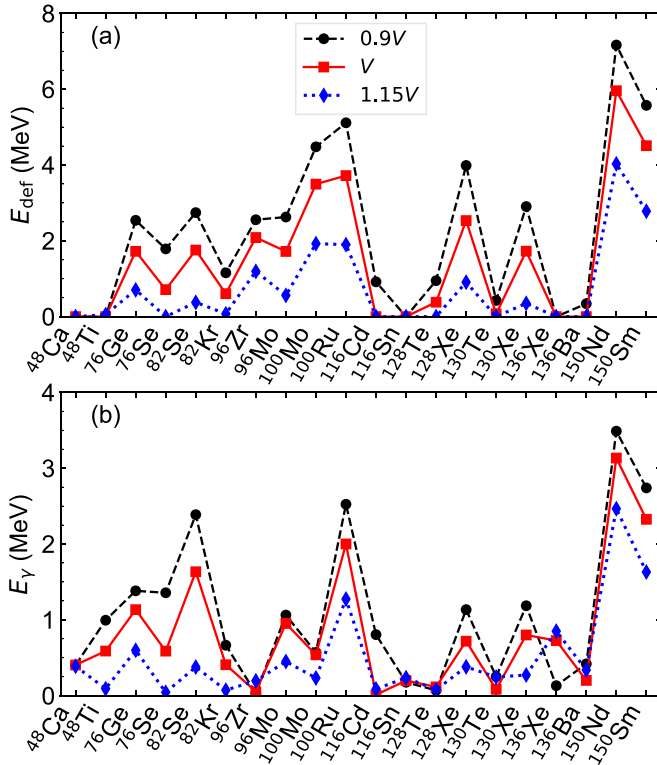
FIG. 3. Energies E_{def} (a) and E_γ extracted from the SCMF PESs for the different pairing strengths. See the main text for the definitions of the above quantities.

ϵ_d and κ parameters are here changed with respect to those with the default V: $\epsilon_d = 0.21$ (0.48) MeV and $\kappa = -0.265$ (-0.21) MeV, for the strength of $0.9V$ ($1.15V$).

3. Low-lying states

Figures 5 and 6 show the excitation energies of the 2_1^+, 4_1^+, 0_2^+, and 2_2^+ states of the initial and final even-even nuclei resulting from the mapped IBM-2, respectively. One sees that the description of the energies for the yrast states 2_1^+ and 4_1^+ is not strongly affected by changing the pairing strength in the underlying RHB-SCMF calculations, except perhaps for the ^{96}Zr and ^{116}Cd nuclei. For the ^{96}Zr nucleus, in particular, there is observed a certain improvement of the description of the 4_1^+ excitation energy. Also for ^{96}Zr, the measured 2_1^+ energy level is particularly high, which is due to the filling of the neutron $d_{5/2}$ subshell. The present IBM-2 cannot reproduce it, since the SCMF PESs for this nucleus with the three pairing choices all suggest a well deformed minimum (see Fig. 1).

As one can see in Figs. 5(c), 5(d), 6(c), and 6(d), dependence of the calculated excitation energies on the choice of the pairing strength is even more visible for the non-yrast states 0_2^+ and 2_2^+. For almost all the even-even nuclei considered, by the increase of the separable pairing force, both the 0_2^+ and 2_2^+ energy levels are generally lowered, and are in some cases in a better agreement with the experimental data [64]. This result is an immediate consequence of the reduced quadrupole-quadrupole interaction strength in the IBM-2 [cf.
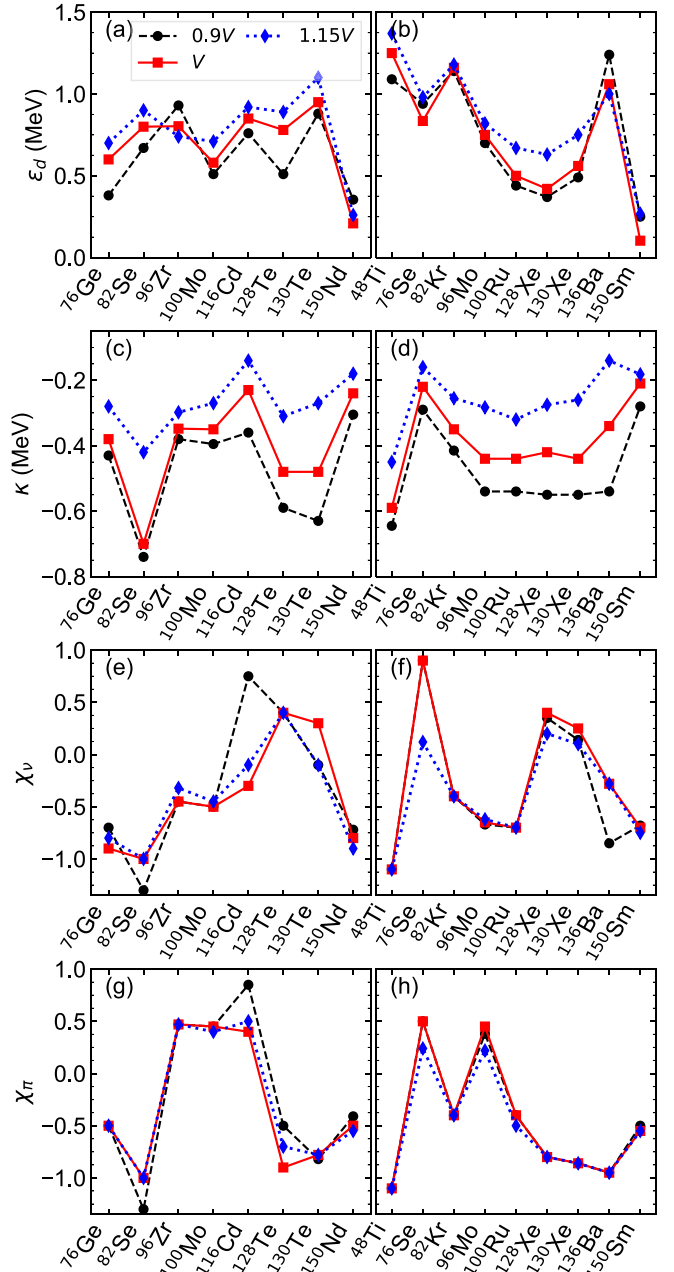

FIG. 4. Derived parameters for the IBM-2 Hamiltonian (3) for the even-even nuclei with the reduced ($0.9V$), default (V), and increased ($1.15V$) strengths of the separable pairing force.

Figs. 4(c) and 4(d)], and further confirms the effect of increasing the pairing strength in the SCMF calculations, which produce the PESs with a potential valley that is much less pronounced.

Significant deviations of the calculated 0_2^+ energy levels from the experimental data are still present, e.g., for ^{100}Mo and ^{150}Nd [Fig. 5(c)], and ^{96}Mo, ^{100}Ru, and ^{150}Sm [Fig. 6(c)], even though the increased pairing strength is considered. Given the fact that these are all predicted to have a well deformed ground state (cf. Figs. 1 and 2), characterized by the large E_{def} energies, perhaps an even larger pairing strength
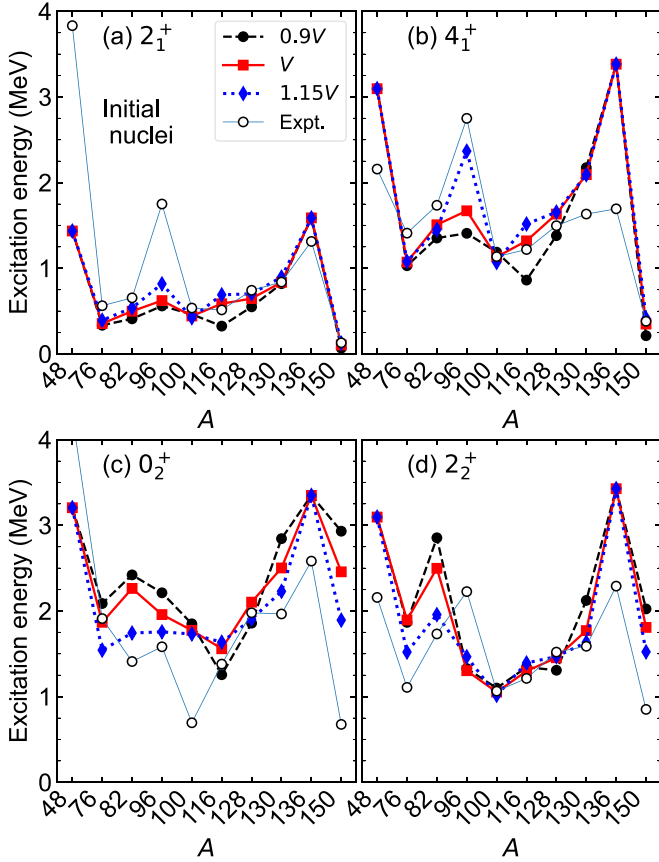
FIG. 5. Excitation energies of the 2_1^+, 4_1^+, 0_2^+, and 2_2^+ states calculated with the mapped IBM-2 for the initial even-even nuclei with the reduced ($0.9V$), default (V), and increased ($1.15V$) pairing strengths in the RHB-SCMF SCMF calculations. Experimental values are taken from the NNDC database [64].

FIG. 6. Same as Fig. 5, but for the final even-even nuclei.

would be required so the PES becomes much more softer, leading to a much weaker quadrupole-quadrupole interaction strength κ for the IBM-2 Hamiltonian. The low-energy 0_2^+ levels, which are supposed to play a part especially in the ^{76}Ge $\rightarrow$ ^{76}Se, ^{100}Mo $\rightarrow$ ^{100}Mo, and ^{150}Nd $\rightarrow$ ^{150}Sm decays, could be adequately handled by the version of the IBM-2 that includes configuration mixing between the normal and intruder states [39]. Within the version of the mapped IBM-2 with a single (normal) configuration as considered here, increasing the pairing strength does not lower the 0_2^+ energy level as dramatically as with the configuration-mixing IBM-2. A more realistic calculation would, therefore, require one to incorporate in the mapping procedure effects of the intruder states by using the configuration-mixing IBM-2, which would be of particular importance for the ^{100}Mo $\rightarrow$ ^{100}Mo(0_2^+) and ^{150}Nd $\rightarrow$ ^{150}Sm(0_2^+) decays.

4. E2 transitions

The $B(E2)$ transition rates for the even-even nuclei are computed in the IBM-2 by using the $E2$ operator

$$\hat{T}_{\mathrm{B}}^{(E2)} = e_\nu^{\mathrm{B}}\hat{Q}_\nu + e_\pi^{\mathrm{B}}\hat{Q}_\pi, \qquad (23)$$

where $\hat{Q}_\rho$ are the same quadrupole operators used in the Hamiltonian (3) with the same value of the χ_ρ parameter. The effective boson charges e_ρ^{B} are here assumed to be the same between neutron and proton systems, $e_\nu^{\mathrm{B}} = e_\pi^{\mathrm{B}} \equiv e^{\mathrm{B}}$, which is then determined so as to reproduce the experimental $B(E2; 2_1^+ \rightarrow 0_1^+)$ value [64] for each nucleus. Figures 7 and 8 display the calculated and experimental $B(E2; 2_1^+ \rightarrow 0_1^+)$, $B(E2; 4_1^+ \rightarrow 2_1^+)$, $B(E2; 0_2^+ \rightarrow 2_1^+)$, and $B(E2; 2_2^+ \rightarrow 2_1^+)$ transition strengths for the even-even nuclei. The calculated $B(E2; 4_1^+ \rightarrow 2_1^+)$ values are, in general, in a good agreement with experiment, and the results from the different pairing strengths are strikingly similar to each other. The $B(E2; 0_2^+ \rightarrow 2_1^+)$ and $B(E2; 2_2^+ \rightarrow 2_1^+)$ transition rates are, however, at variance between the calculations with different pairing strengths. A significant improvement of the description of the $B(E2; 2_2^+ \rightarrow 2_1^+)$ transition rate due to the increase of the pairing force is observed for ^{76}Se. The modification of the separable pairing strength thus appears to affect the wave functions for the even-even nuclei, especially those of the non-yrast states.

B. Intermediate odd-odd nuclei

Figure 9 depicts the calculated excitation energies of low-spin positive-parity states of the intermediate odd-odd nuclei resulting from the IBFFM-2 with the three different pairing strengths. The correct ground-state spin is reproduced by any
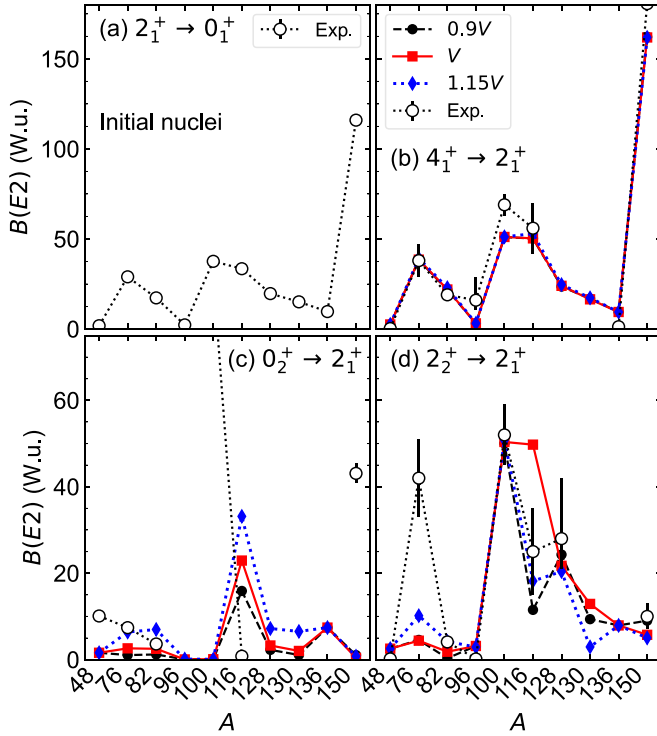
FIG. 7. $B(E2)$ values [in Weisskopf units (W.u.)] for the $E2$ transitions (a) $2_1^+ \rightarrow 0_1^+$, (b) $4_1^+ \rightarrow 2_1^+$, (c) $0_2^+ \rightarrow 2_1^+$, and (d) $2_2^+ \rightarrow 2_1^+$ calculated for the initial even-even nuclei by using the reduced ($0.9V$), default (V), and increased ($1.15V$) pairing strengths. Experimental data are adopted from the NNDC database. Note that since the effective boson charges are fit to the experimental $B(E2; 2_1^+ \rightarrow 0_1^+)$ values [64], the calculated values for this transition are not included in the plot.
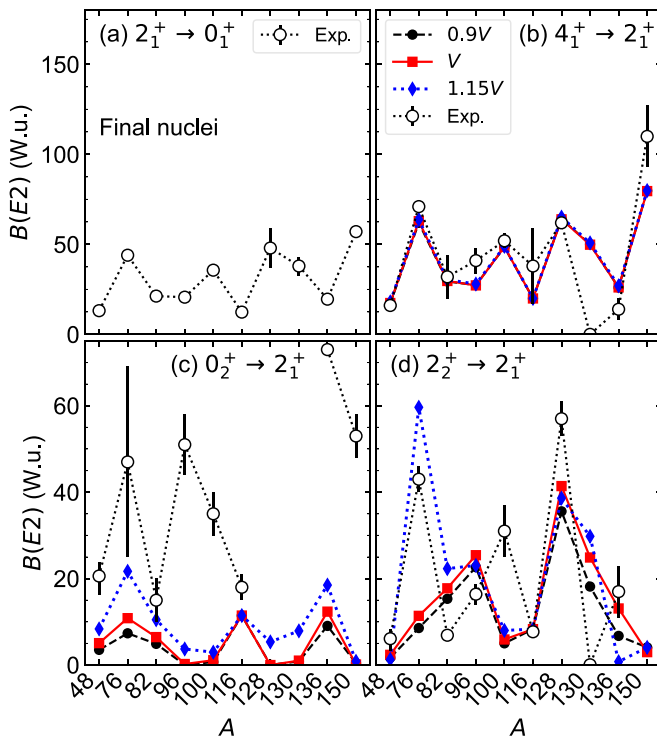

FIG. 8. Same as Fig. 7, but for the final even-even nuclei.
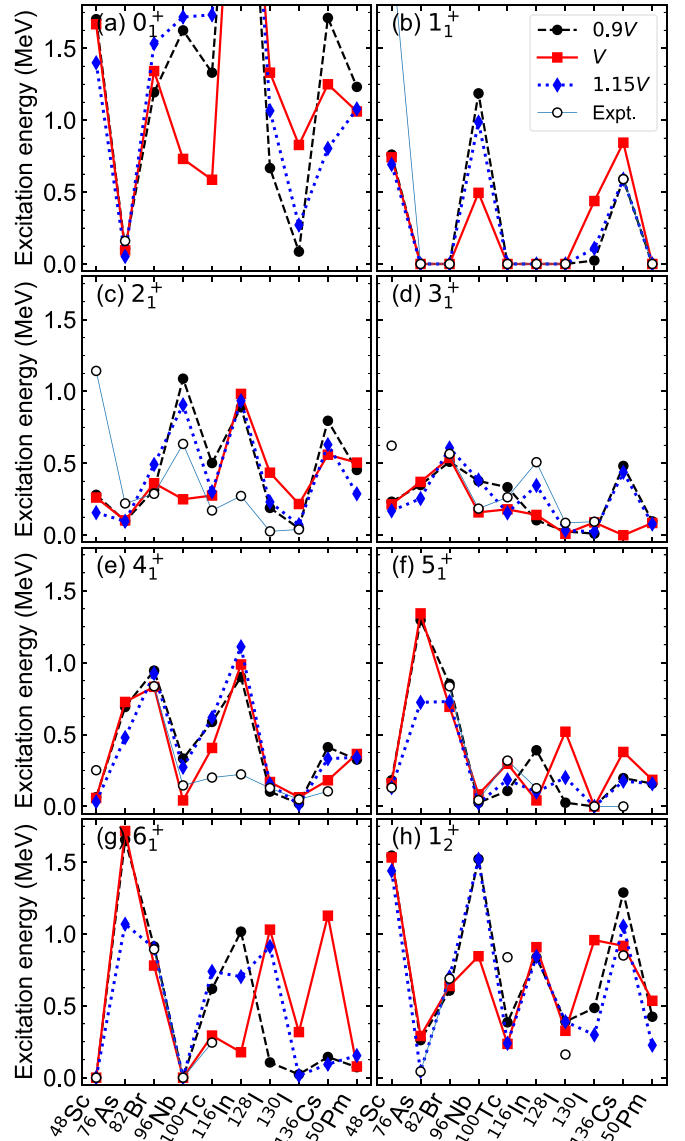
FIG. 9. Excitation energies of the 0_1^+, 1_1^+, 2_1^+, 3_1^+, 4_1^+, 5_1^+, 6_1^+, and 1_2^+ states calculated with the IBFFM-2 for the intermediate odd-odd nuclei with the pairing strengths of $0.9V$, V, and $1.15V$. Experimental data are taken from the NNDC database [64].

of the three IBFFM-2 calculations, except for the ^{136}Cs nucleus. One can see that the IBFFM-2 descriptions based on the three choices of the pairing strength are rather different from each other. There appears to be, however, no general tendency of reaching a better agreement with the experimental data by changing the pairing strength in either way. The differences in the calculated energy levels due to the choices of the pairing strength are primarily attributed to the differences between the respective IBFFM-2 parameters, which, e.g., in ^{96}Nb, ^{128}I, and ^{130}I, differ significantly from each other (see Table VIII in the Appendix).

Furthermore, the $E2$ and $M1$ transition properties for the odd-odd nuclei are studied. The $E2$ operator is given by

$$\hat{T}^{(E2)} = \hat{T}_{\mathrm{B}}^{(E2)} + \hat{T}_{\mathrm{F}}^{(E2)}, \qquad (24)$$

TABLE II. GT and F matrix elements obtained from the mapped IBM-2 based on the separable pairing strengths of $0.9V$, V, and $1.15V$ in the RHB-SCMF calculations for the $0_1^+ \to 0_1^+ 2\nu\beta\beta$ decays of the candidate nuclei.

$0_1^+ \to 0_1^+$ decay	$M_{2\nu}^{\mathrm{GT}}$			$M_{2\nu}^{\mathrm{F}}$		
	$0.9V$	V	$1.15V$	$0.9V$	V	$1.15V$
$^{48}\mathrm{Ca} \to {}^{48}\mathrm{Ti}$	0.060	0.031	0.077	0.029	0.016	−0.018
$^{76}\mathrm{Ge} \to {}^{76}\mathrm{Se}$	0.024	0.036	−0.128	0.000	−0.002	0.059
$^{82}\mathrm{Se} \to {}^{82}\mathrm{Kr}$	0.024	−0.052	0.131	0.000	0.011	−0.045
$^{96}\mathrm{Zr} \to {}^{96}\mathrm{Mo}$	−0.087	0.175	−0.159	−0.000	0.001	−0.000
$^{100}\mathrm{Mo} \to {}^{100}\mathrm{Ru}$	0.465	0.483	0.574	−0.005	−0.000	−0.000
$^{116}\mathrm{Cd} \to {}^{116}\mathrm{Sn}$	−0.225	0.275	0.337	−0.000	0.000	−0.001
$^{128}\mathrm{Te} \to {}^{128}\mathrm{Xe}$	0.035	−0.102	0.073	−0.007	0.005	−0.041
$^{130}\mathrm{Te} \to {}^{130}\mathrm{Xe}$	0.008	−0.038	−0.118	−0.006	0.023	0.076
$^{136}\mathrm{Xe} \to {}^{136}\mathrm{Ba}$	−0.091	−0.102	−0.232	−0.004	0.029	0.099
$^{150}\mathrm{Nd} \to {}^{150}\mathrm{Sm}$	0.299	−0.369	−0.501	−0.000	0.000	0.000

with the boson operator $\hat{T}_{\mathrm{B}}^{(E2)}$ defined in Eq. (23), and the fermion one

$$
\hat{T}_{\mathrm{F}}^{(E2)} = -\frac{1}{\sqrt{5}} \sum_{\rho=\nu,\pi} \sum_{j_\rho j_\rho'} \left(u_{j_\rho} u_{j_\rho'} - v_{j_\rho} v_{j_\rho'} \right)
$$
$$
\times \left\langle \ell_\rho \frac{1}{2} j_\rho \left\| e_\rho^{\mathrm{F}} r^2 Y^{(2)} \right\| \ell_\rho' \frac{1}{2} j_\rho' \right\rangle \left(a_{j_\rho}^\dagger \times \tilde{a}_{j_\rho'} \right)^{(2)}. \quad (25)
$$

The neutron and proton effective charges, $e_\nu^{\mathrm{F}} = 0.5\,eb$ and $e_\pi^{\mathrm{F}} = 1.5\,eb$, are taken from Ref. [27]. The $M1$ transition operator $\hat{T}^{(M1)}$ reads

$$
\hat{T}^{(M1)} = \sqrt{\frac{3}{4\pi}} \sum_{\rho=\nu,\pi} \left[g_\rho^{\mathrm{B}} \hat{L}_\rho - \frac{1}{\sqrt{3}} \sum_{j_\rho j_\rho'} \left(u_{j_\rho} u_{j_\rho'} + v_{j_\rho} v_{j_\rho'} \right) \right.
$$
$$
\left. \times \langle j_\rho \| g_l^\rho \ell + g_s^\rho \mathbf{s} \| j_\rho' \rangle \left(a_{j_\rho}^\dagger \times \tilde{a}_{j_\rho'} \right)^{(1)} \right], \quad (26)
$$

where $\hat{L}_\rho$ is the angular momentum operator in the boson system (3), and the empirical g factors for the neutron and proton bosons, $g_\nu^{\mathrm{B}} = 0\mu_N$ and $g_\pi^{\mathrm{B}} = 1.0\mu_N$, respectively, are considered. For the neutron (or proton) g factors, the free values $g_\ell^\nu = 0\mu_N$ and $g_s^\nu = -3.82\mu_N$ ($g_\ell^\pi = 1.0\mu_N$ and $g_s^\pi = 5.58\mu_N$) are employed, with g_s^ρ quenched by 30%.

Table I gives the calculated electric quadrupole $Q(I)$ and magnetic dipole $\mu(I)$ moments and $B(M1)$ transition probabilities in the cases of the three different pairing strengths in the RHB-SCMF calculations in comparison with the available experimental data [64,66]. The transition properties appear to be sensitive to the choice of the pairing strength. Notable difference is found in the $\mu(1_1^+)$ and $\mu(6_1^+)$ moments for the $^{76}\mathrm{As}$ and $^{96}\mathrm{Nb}$ nuclei, respectively, since not only their magnitudes but also signs are different between the pairing strengths considered.

The IBFFM-2 wave function for the 1_1^+ ground state of $^{76}\mathrm{As}$ is here accounted for by the mixture of the neutron-proton pair components $[\nu p_{1/2} \otimes \pi p_{3/2}]^{(J=1^+)}$ (45%), and $[\nu p_{1/2} \otimes \pi f_{5/2}]^{(J=5^+)}$ (38%) when the default (V) and reduced ($0.9V$) pairing strengths are employed in the RHB-SCMF calculations. For the increased pairing ($1.15V$), the

dominant configuration is of the type $[\nu p_{1/2} \otimes \pi p_{3/2}]^{(J=1^+)}$ (72%), and there are numerous minor contributions from other pair components. Since the compositions of the 1_1^+ wave function and the employed boson-fermion and fermion-fermion interaction parameters are similar between the IBFFM-2 calculations with V and $0.9V$, the difference between the $\mu(1_1^+)$ values from the two calculations probably arises from the difference between the even-even boson-core ($^{76}\mathrm{Ge}$) parameters. Concerning the $^{96}\mathrm{Nb}$ nucleus, the IBFFM-2 wave function of the 6_1^+ ground state is mostly (86%) composed of the pair configuration $[\nu d_{5/2} \otimes \pi g_{9/2}]^{(J=6^+)}$ in the case of the default pairing strength (V). In those calculations in which reduced ($0.9V$) and increased ($1.15V$) pairing strengths are employed, however, the pair component of the type $[\nu h_{11/2} \otimes \pi p_{1/2}]^{(J=6^+)}$ makes a dominant (89%, and 87%, respectively) contribution to the the IBFFM-2 6_1^+ wave functions.

The differences in the nature of the wave functions and the calculated electromagnetic transition properties for the odd-odd nuclei among the three cases of the pairing strength arise from the differences in the parameters involved in the IBFFM-2 Hamiltonian, which are especially dependent on the strength parameters for the even-even boson core. One cannot draw any definite conclusion from Table I that increasing or reducing the pairing strength in the RHB-SCMF model is particularly good for describing many of the electromagnetic transition properties of the odd-odd nuclei studied. It appears to be rather reasonable to use the standard pairing strength V, since only in that case is a reasonable description obtained for the $\mu(1_1^+)$ and $\mu(1_6^+)$ moments of $^{76}\mathrm{As}$ and $^{96}\mathrm{Nb}$, respectively (cf. Table I).

IV. $2\nu\beta\beta$ DECAY

A. GT and F transitions

Tables II and III present the calculated $M_{2\nu}^{\mathrm{GT}}$ (19) and $M_{2\nu}^{\mathrm{F}}$ (20) for the ground-state-to-ground-state ($0_1^+ \to 0_1^+$), and for the ground-state-to-first-excited state ($0_1^+ \to 0_2^+$) decays, respectively. As can be seen in Tables II and III, by the increase of the pairing strength the predicted $M_{2\nu}^{\mathrm{GT}}$ value for the

TABLE III. Same as Table II, but for the $0_1^+ \to 0_2^+$ $2\nu\beta\beta$ decay.

$0_1^+ \to 0_2^+$ decay	$M_{2\nu}^{\mathrm{GT}}$			$M_{2\nu}^{\mathrm{F}}$		
	0.9V	V	1.15V	0.9V	V	1.15V
^{48}Ca $\to$ ^{48}Ti	0.037	0.069	0.024	−0.103	−0.068	−0.068
^{76}Ge $\to$ ^{76}Se	−0.056	0.064	−0.100	0.032	−0.036	0.094
^{82}Se $\to$ ^{82}Kr	−0.074	0.090	0.168	0.039	−0.055	−0.092
^{96}Zr $\to$ ^{96}Mo	0.038	−0.068	0.052	0.000	−0.001	0.001
^{100}Mo $\to$ ^{100}Ru	0.269	0.154	0.054	−0.001	0.000	−0.000
^{116}Cd $\to$ ^{116}Sn	0.106	−0.035	0.118	0.001	−0.001	−0.003
^{128}Te $\to$ ^{128}Xe	−0.027	0.032	−0.134	0.024	0.002	0.112
^{130}Te $\to$ ^{130}Xe	0.092	0.037	0.363	−0.052	−0.018	−0.232
^{136}Xe $\to$ ^{136}Ba	0.045	0.009	−0.027	0.022	−0.000	−0.000
^{150}Nd $\to$ ^{150}Sm	0.095	−0.207	0.156	0.000	−0.000	0.000

$0_1^+ \to 0_1^+$ decay generally increases in magnitude. This is also true for the $M_{2\nu}^{\mathrm{F}}$ values. For some of the studied $2\nu\beta\beta$ decays, the absolute value $|M_{2\nu}^{\mathrm{F}}|$ is so large as to be in the same order of magnitude as $|M_{2\nu}^{\mathrm{GT}}|$. This was already pointed out in the previous mapped IBM-2 study of Ref. [27], and appears to occur irrespective of which pairing strength is considered in the present analysis. This is so for those $2\nu\beta\beta$ decays in which the neutrons and protons are in the same major oscillator shell so that the Fermi transitions are allowed. For the ^{48}Ca $\to$ ^{48}Ti decay in particular, the $|M_{2\nu}^{\mathrm{F}}|$ value is equal to or even larger than $|M_{2\nu}^{\mathrm{GT}}|$. The large $|M_{2\nu}^{\mathrm{F}}|/|M_{2\nu}^{\mathrm{GT}}|$ ratio indicates that there is a spurious isospin symmetry breaking that is not expected in the $2\nu\beta\beta$ decay. Effective ways to restore the isospin symmetry would be, for instance, to simply discard $M_{2\nu}^{\mathrm{F}}$ in the calculations of $M_{2\nu}$, and to make some modifications to the Fermi transition operator (15) so that the Fermi matrix elements should vanish in the closure approximation (see Refs. [67,68] for detailed discussions). In the present study, no such treatment is made to restore the isospin symmetry broken in the employed model.

It should be mentioned that the results in the case of the default pairing strength V are found in Table III of Ref. [27], and that one can notice slight deviations of the present $M_{2\nu}^{\mathrm{GT}}$ and $M_{2\nu}^{\mathrm{F}}$ values from those in the previous study [27] in some instances. This is mainly due to the following differences between the present calculation and that of [27]. First, as already mentioned, in some of the even-even and odd-odd nuclei modifications to the IBM-2 as well as IBFFM-2 parameters are made in the present calculation employing the same default pairing strength as in Ref. [27]. Second, in the present IBFFM-2 calculation the maximum number of iterations in the numerical (Lanczos) diagonalization of the IBFFM-2 Hamiltonian is set to be 200 000 times for all the odd-odd nuclei and in all the three cases of the separable pairing strength, whereas in Ref. [27] the number of iterations was much less and also at variance with the nuclei. Third, the truncation of the maximum energy for the intermediate states for the calculations of $M_{2\nu}^{\mathrm{GT}}$ and $M_{2\nu}^{\mathrm{F}}$ is here set to be 30 MeV, while in [27] it was 10 MeV. These modifications, especially the second and third ones, could have affected the predictions of the $M_{2\nu}^{\mathrm{GT}}$, as well as $M_{2\nu}^{\mathrm{F}}$, and hence $M_{2\nu}$ values

since these quantities require to include contributions from higher-lying intermediate states, which should be sensitive to the convergence of the IBFFM-2 eigenvalues and to the truncation to their energy range.

Figure 10 depicts the running sums of the $M_{2\nu}^{\mathrm{GT}}$ (19) and $M_{2\nu}^{\mathrm{F}}$ (20) matrix elements for the $0_1^+ \to 0_1^+$ $2\nu\beta\beta$ decays as functions of the excitation energies $E(1_N^+)$ and $E(0_N^+)$ of the intermediate states, respectively. The GT sums in most cases appear to be accounted for by the contributions from the lower-lying 1^+ states, typically below $E(1_N^+) \approx 3$ MeV. This result is consistent with the so-called single-state dominance (SSD) [69,70] or low-lying-state dominance (LLSD) [71] hypotheses drawn from the pnQRPA studies for the $2\nu\beta\beta$ decay. The behaviors of the GT sums are also at variance with the calculations employing the different pairing strengths in the RHB-SCMF input, with representative cases being the ^{116}Cd and ^{150}Nd decays. Among the three IBM-2 results, the GT running sums resulting from the increased pairing strength 1.15V exhibit the strongest dependence on the 1^+ excitation energies so that they continue to increase in magnitude, implying that contributions from higher-lying intermediate states are more important than in the calculations with weaker pairing forces.

Regarding the Fermi transitions, in the majority of the considered decay processes the contributions from the low-lying 0_N^+ states, with typically up to $E(0_N^+) \approx 5$ MeV, determine most of the $M_{2\nu}^{\mathrm{F}}$ matrix element. The Fermi running sums seem to show a stronger dependence on the intermediate energies than the GT sums. Peculiar behaviors of the calculated Fermi sums are found for the ^{128}Te, ^{130}Te, and ^{136}Xe decays, where especially the sums obtained with the reduced pairing strength 0.9V decrease in magnitude with $E(0_N^+)$.

B. $2\nu\beta\beta$ NMEs

Figure 11 displays the calculated $M_{2\nu}$ (21) for the $0_1^+ \to 0_1^+$ $2\nu\beta\beta$ decay for the considered nuclei. The $M_{2\nu}$ values calculated for the $0_1^+ \to 0_1^+$ $2\nu\beta\beta$ decays, and those for the ^{100}Mo(0_1^+) $\to$ ^{100}Ru(0_2^+) and ^{150}Nd(0_1^+) $\to$ ^{150}Sm(0_2^+) decays are listed from the second to fourth columns of Table IV. The experimental data [13] included both in the
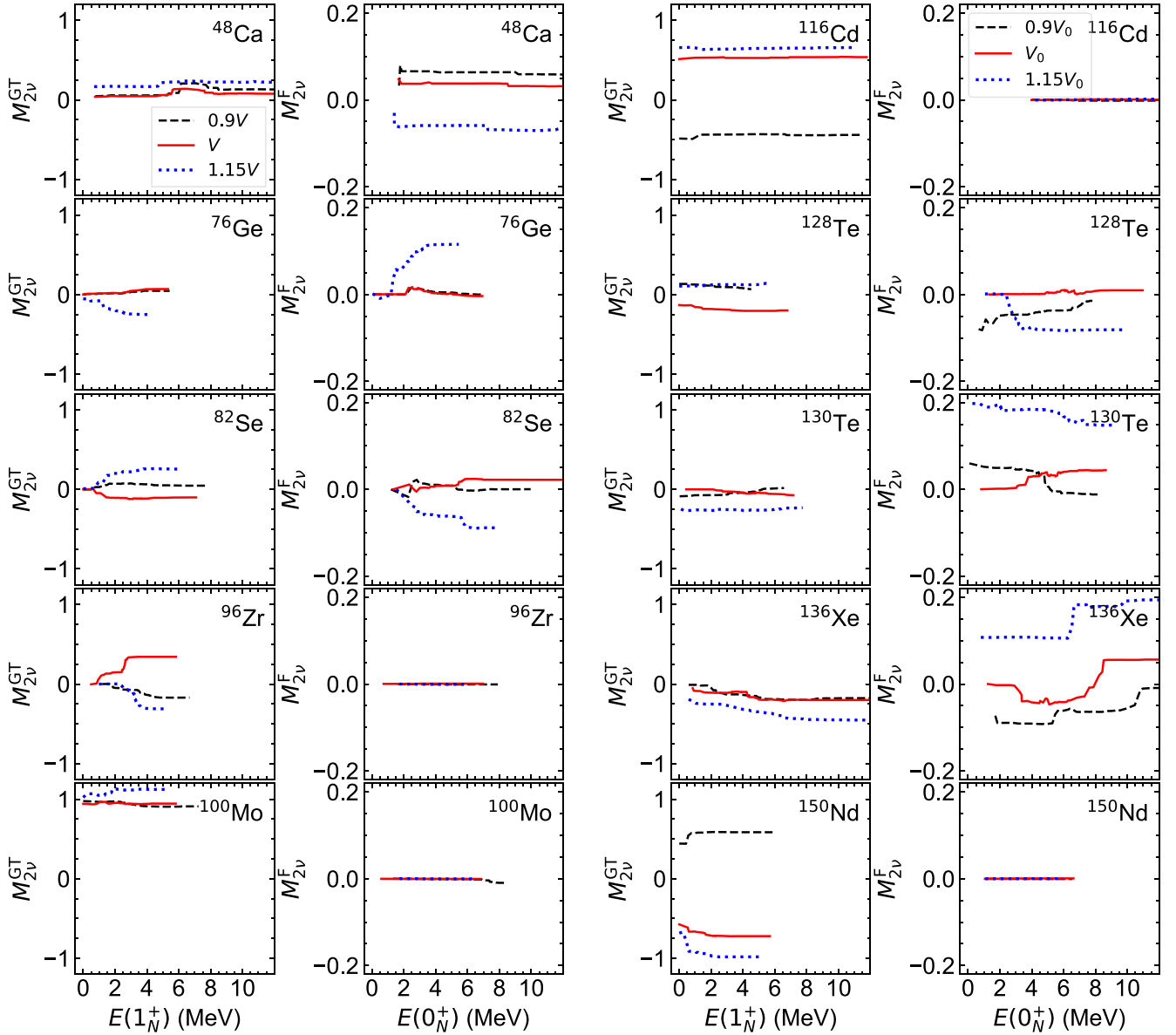
FIG. 10. Running sums of the GT (19) (first and third columns) and F (20) (second and fourth columns) transition strengths for the $2\nu\beta\beta$ decay of the candidate even-even nuclei as functions of the excitation energies of the 1_N^+ and 0_N^+ intermediate states. The calculated results with the reduced, default, and increased pairing strengths employed in the RHB-SCMF calculations are compared.

figure and table are those extracted from the measured half-lives with the phase-space factors $G_{2\nu}$ taken from Ref. [65], and are referred to as "Recommended Value" in Table III of Ref. [13].

As is evident from Fig. 11, the predicted $|M_{2\nu}|$ values with the bare (unquenched) g_A factor are, in most cases, substantially larger than the experimental values regardless of which pairing strength is used in the RHB-SCMF calculations, illustrative cases being the ^{100}Mo $\rightarrow$ ^{100}Ru, ^{116}Cd $\rightarrow$ ^{116}Sn, and ^{150}Nd $\rightarrow$ ^{150}Sm decays. For the ^{48}Ca $\rightarrow$ ^{48}Ti, ^{76}Ge $\rightarrow$ ^{76}Se, and ^{82}Se $\rightarrow$ ^{82}Kr decays, in contrast, the predicted $|M_{2\nu}|$ with the default pairing strength V are approximately equal to or even lower than the experimental $|M_{2\nu}^{\text{eff}}|$ values. A remarkable finding in Fig. 11 is that, when the increased pairing

strength is adopted, the $|M_{2\nu}|$ values systematically become larger.

In the last two rows of Table IV the $0_1^+ \rightarrow 0_2^+$ decay $|M_{2\nu}|$ values are also shown for the ^{100}Mo and ^{150}Nd, for which experimental data [13] are available. As compared to the $|M_{2\nu}(0_1^+ \rightarrow 0_1^+)|$ values, which exhibit an increase with the enhanced pairing force, one can hardly see a general trend of the $|M_{2\nu}(0_1^+ \rightarrow 0_2^+)|$ values for the ^{100}Mo and ^{150}Nd decays due to the modification of the pairing strength.

To make a more reasonable comparison with experiment, effective g_A factors, denoted as g_A^{eff}, are considered. As in the previous mapped IBM-2 study [27], while both g_V and ratio g_V/g_A in Eq. (21) remain unchanged, only the g_A factor is

TABLE IV. Predicted $|M_{2\nu}|$ obtained from the mapped IBM-2 employing the separable pairing force with the reduced ($0.9V$), default (V), and increased ($1.15V$) strengths. From the second to fourth columns are $|M_{2\nu}|$ values obtained with the bare g_A factor, and from the fifth to seventh columns are those with the effective g_A^{eff} factor defined in Eq. (28). The effective $|M_{2\nu}^{\text{eff}}|$ extracted from the experimental $2\nu\beta\beta$ half-lives [13] are shown in the eighth column.

Decay	$|M_{2\nu}|$ with g_A			$|M_{2\nu}|$ with g_A^{eff}			
	$0.9V$	V	$1.15V$	$0.9V$	V	$1.15V$	$|M_{2\nu}^{\text{eff}}|$
$^{48}\text{Ca} \to {}^{48}\text{Ti}$	0.068	0.033	0.142	0.067	0.030	0.069	0.035 ± 0.003
$^{76}\text{Ge} \to {}^{76}\text{Se}$	0.038	0.060	0.265	0.027	0.032	0.083	0.106 ± 0.004
$^{82}\text{Se} \to {}^{82}\text{Kr}$	0.038	0.095	0.256	0.025	0.046	0.072	0.085 ± 0.001
$^{96}\text{Zr} \to {}^{96}\text{Mo}$	0.140	0.281	0.256	0.078	0.107	0.058	0.088 ± 0.004
$^{100}\text{Mo} \to {}^{100}\text{Ru}$	0.754	0.778	0.925	0.401	0.275	0.197	0.185 ± 0.002
$^{116}\text{Cd} \to {}^{116}\text{Sn}$	0.361	0.442	0.543	0.159	0.117	0.089	0.108 ± 0.003
$^{128}\text{Te} \to {}^{128}\text{Xe}$	0.063	0.169	0.159	0.024	0.036	0.022	0.043 ± 0.003
$^{130}\text{Te} \to {}^{130}\text{Xe}$	0.020	0.083	0.265	0.007	0.017	0.035	0.0293 ± 0.0009
$^{136}\text{Xe} \to {}^{136}\text{Ba}$	0.141	0.194	0.472	0.049	0.036	0.056	0.0181 ± 0.0006
$^{150}\text{Nd} \to {}^{150}\text{Sm}$	0.482	0.594	0.808	0.141	0.085	0.077	0.055 ± 0.003
$^{100}\text{Mo} \to {}^{100}\text{Ru}(0_2^+)$	0.434	0.248	0.086	0.231	0.088	0.018	0.151 ± 0.004
$^{150}\text{Nd} \to {}^{150}\text{Sm}(0_2^+)$	0.153	0.333	0.251	0.045	0.048	0.024	0.044 ± 0.005

modified in such a way that

$$M_{2\nu} \to M_{2\nu}^{\text{eff}} = \left(\frac{g_A^{\text{eff}}}{g_A}\right)^2 M_{2\nu}. \quad (27)$$

The quenching factor q is also extracted from the above relation, $q = g_A^{\text{eff}}/g_A$. The g_A^{eff} is here assumed to be a smooth function of the mass number A, and the following functional form was shown [27] to give an overall good description of the experimental NMEs:

$$g_A^{\text{eff}} = ce^{-dA}, \quad (28)$$

with c and d being numerical constants that are fitted to the experimental $M_{2\nu}^{\text{eff}}$ values [13]. Note the constant $c = g_A$ in Ref. [27].

Figure 12 exhibits those g_A^{eff} values (shown as solid symbols connected by thin solid lines) that would be required so that the calculated $M_{2\nu}^{\text{eff}}$'s agree with the data. The g_A^{eff} values corresponding to the pairing strengths of $0.9V$ and
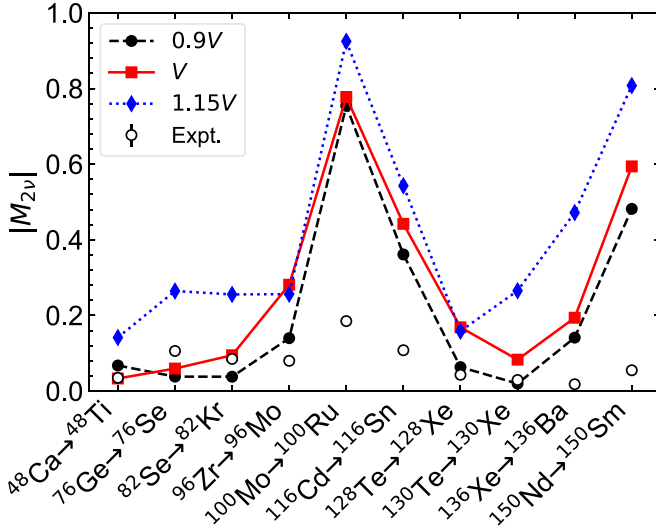

FIG. 11. Calculated NMEs $M_{2\nu}$ for the considered $2\nu\beta\beta$ decays, obtained from the mapped IBM-2 employing the three different pairing strengths ($0.9V$, V, and $1.15V$) in the RHB-SCMF calculations. The bare g_A factor is employed, hence no quenching is made. Experimental $M_{2\nu}$, extracted from the measured half-lives, are taken from Ref. [13].
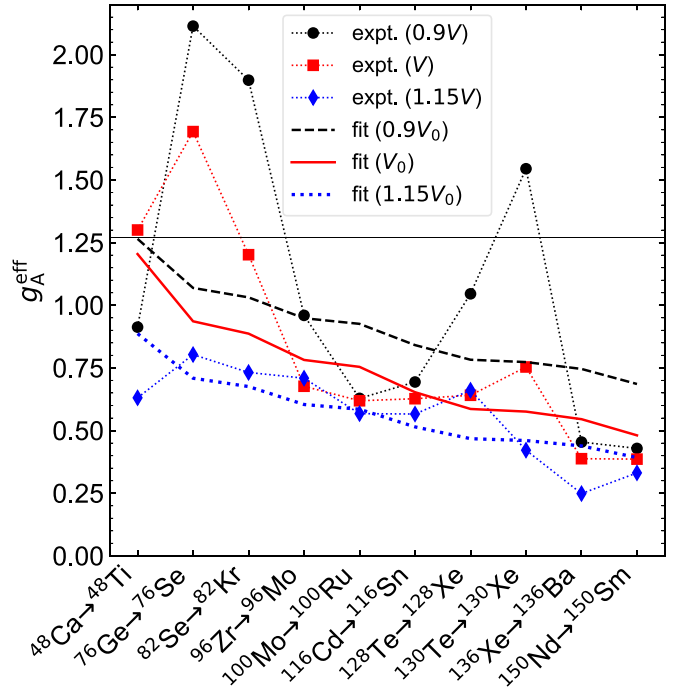

FIG. 12. Effective g_A^{eff} factors that are required to reproduce the experimental $|M_{2\nu}^{\text{eff}}|$ values (denoted by "expt."), and the mass-dependent g_A^{eff} factors (denoted by "fit") obtained by using the formula Eq. (28), for the different pairing strengths in the RHB-SCMF calculations. The free-nucleon value g_A is indicated by the sold horizontal line.
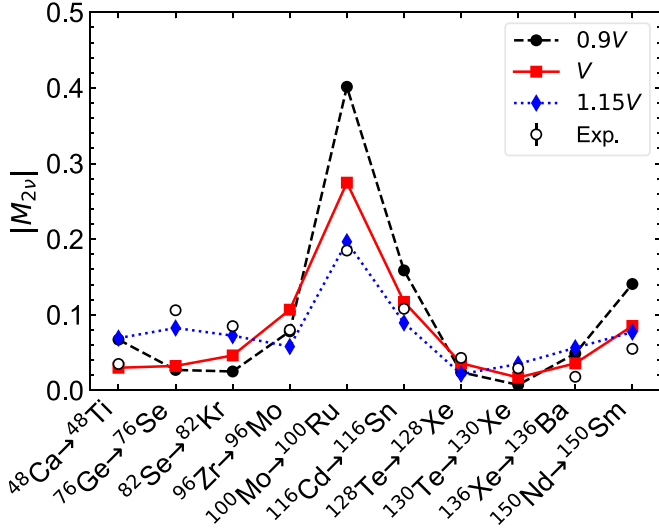
FIG. 13. Effective NMEs $|M_{2\nu}^{\text{eff}}|$ calculated by using the g_A^{eff} factors defined in Eq. (28) in the cases of the three different pairing strengths.

V appear to be significantly at variance with the different decay processes, and those for ^{76}Ge, ^{82}Se, and ^{130}Te decays are particularly large, being close to or much larger than the bare value, $g_A = 1.269$, represented by the horizontal solid line in the figure. On the other hand, the g_A^{eff} values that are expected for the calculated $M_{2\nu}$ result with the increased pairing strength $1.15V$ change smoothly as functions of the mass A.

The function (28) is then fitted to those effective g_A values extracted from the data for each nucleus, giving rise to the numerical constants c and d as $(c, d) = (1.69, 0.006)$, $(1.86, 0.009)$, and $(1.30, 0.008)$ for the calculations with the pairing strengths of $0.9V$, V, and $1.15V$, respectively. Note that the free nucleon value $g_A = 1.269$ at $A = 1$ is included in the fit. The fitted g_A^{eff}'s (depicted as the thick lines in Fig. 12) do exhibit smoothly decreasing systematic as functions of A for all the three pairing strengths, with the corresponding values for the masses $A = 48$ to 150 changing within the ranges $g_A^{\text{eff}} = 1.26$–0.69 (with $0.9V$), 1.20–0.48 (with V), and 0.89–0.39 (with $1.15V$). The quenching factors q estimated for the masses $A = 48$ to 150 also decrease monotonously in the intervals $q = 1.00-0.54$, $0.95-0.38$, and $0.70-0.31$, for the calculations with the reduced $(0.9V)$, default (V), and increased $(1.15V)$ pairing strengths, respectively. Figure 13 depicts the resultant $|M_{2\nu}^{\text{eff}}|$ values, which are computed by using the effective g_A^{eff} (28) determined by the aforementioned procedure, and compare them with the experimental data [13]. As one can see, while certain improvements appear to be made by using the increased pairing strength $1.15V$, particularly for the ^{76}Ge, ^{82}Se, and ^{100}Mo decays, the calculations with the original pairing strength V provide an overall good description of the observed $|M_{2\nu}^{\text{eff}}|$ values. The calculated results with the reduced pairing strength $0.9V$ seem to be, in many cases, rather far from the experimental data.

The predicted $|M_{2\nu}^{\text{eff}}|$ with the effective g_A^{eff}, which are shown in Fig. 13, are also listed from the fifth to seventh columns of Table IV. The table also gives results for the $|M_{2\nu}^{\text{eff}}(0_1^+ \to 0_2^+)|$ NMEs for the ^{100}Mo and ^{150}Nd decays, for which the same g_A^{eff} values as those used for the $|M_{2\nu}^{\text{eff}}(0_1^+ \to 0_1^+)|$ ones are employed. Smaller $|M_{2\nu}^{\text{eff}}(0_1^+ \to 0_1^+)|$ are obtained with the stronger pairing interaction, reflecting that the larger quenching is expected from the systematic of the unquenched $|M_{2\nu}|$ calculated with the increased pairing strength. Note, however, that the use of the same g_A^{eff} values for the $0_1^+ \to 0_1^+$ and $0_1^+ \to 0_2^+$ decays may not be entirely justified, that is, some different quenching may need to be made for the decays to the different final states.

C. Half-lives

The calculated $2\nu\beta\beta$-decay half-lives $\tau_{1/2}^{(2\nu)}$ (22), with the NMEs $|M_{2\nu}|$ given in Table IV, are listed in Table V. The experimental data [13], shown in the eighth column, correspond to those that are referred to as "Average (or Recommended) value" in Table I of Ref. [13], which are based on the measured $2\nu\beta\beta\tau_{1/2}^{(2\nu)}$ from the 1990s till 2020. As in the case of the $|M_{2\nu}^{\text{eff}}|$ results in Fig. 13, the calculations with the default pairing strength V provide an overall good description of the $\tau_{1/2}^{(2\nu)}$ data, with $M_{2\nu}$ quenched with the effective g_A^{eff} factors of Eq. (28). Increasing the pairing strength to $1.15V$ leads to some improvements in specific cases of the ^{76}Ge $\to ^{76}$Se, ^{82}Se $\to ^{82}$Kr, and ^{100}Mo $\to ^{100}$Ru decays. As for the $\tau_{1/2}^{(2\nu)}$'s for the ^{136}Xe $\to ^{136}$Ba and ^{100}Mo $\to ^{100}$Ru(0_2^+) decays, however, enhancing the pairing does not seem to work well, as the predicted $\tau_{1/2}^{(2\nu)}$'s are here by about one and two orders of magnitude shorter and longer, respectively, than the experimental ones. It should be worth mentioning more recent measurements of the $2\nu\beta\beta$-decay $\tau_{1/2}^{(2\nu)}$ concerning some of the candidate nuclei: a GERDA experiment for the ^{76}Ge decay [14] obtained $\tau_{1/2}^{(2\nu)} = (2.022 \pm 0.018_{\text{stat}} \pm 0.038_{\text{syst}}) \times 10^{21}$ yr, CUPID-Mo experiments on the ^{100}Mo decay reported $\tau_{1/2}^{(2\nu)} = [7.07 \pm 0.02(\text{stat}) \pm 0.11(\text{syst})] \times 10^{18}$ yr for the $0_1^+ \to 0_1^+$ transition [15], and $[7.5 \pm 0.8(\text{stat})_{-0.3}^{+0.4}] \times 10^{20}$ yr for the $0_1^+ \to 0_2^+$ transition [16], and a CUORE measurement on ^{130}Te [17] provided $\tau_{1/2}^{(2\nu)} = [7.71_{-0.06}^{+0.08}(\text{stat})_{-0.15}^{+0.12}(\text{syst})] \times 10^{20}$ yr. All these new entries present crucial updates on the $2\nu\beta\beta$-decay $\tau_{1/2}^{(2\nu)}$ data with high accuracy, and are more or less close to the average values of Ref. [13] listed in Table V.

Concerning the ^{100}Mo and ^{150}Nd decays, ratios of the measured $\tau_{1/2}^{(2\nu)}$ values for the $0_1^+ \to 0_1^+$ to $0_1^+ \to 0_2^+$ decays are computed as

$$\frac{\tau_{1/2}^{(2\nu)}[^{100}\text{Mo}(0_1^+) \to ^{100}\text{Ru}(0_2^+)]}{\tau_{1/2}^{(2\nu)}[^{100}\text{Mo}(0_1^+) \to ^{100}\text{Ru}(0_1^+)]} = 94.9_{-5.9}^{+7.4}, \quad (29)$$

while the predicted ratios in the present calculation are much larger: 165, 536, and 6279, obtained for the pairing strengths of $0.9V$, V, and $1.15V$, respectively. The experimental ratio

TABLE V. Calculated $2\nu\beta\beta$-decay $\tau_{1/2}^{(2\nu)}$'s (22) (in year) with the unquenched g_A factor (from the second to fourth columns), and with the effective g_A^{eff} factors defined in Eq. (28) (from the fifth to seventh columns) obtained from the mapped IBM-2 with the different pairing strengths $0.9V$, V, and $1.15V$. The experimental $\tau_{1/2}^{(2\nu)}$ [13] are included in the eighth column.

| | $\tau_{1/2}^{(2\nu)}$ (yr), with g_A | | | $\tau_{1/2}^{(2\nu)}$ (yr), with g_A^{eff} | | | |
Decay	0.9V	V	1.15V	0.9V	V	1.15V	Experiment
$^{48}\mathrm{Ca} \to {}^{48}\mathrm{Ti}$	1.41×10^{19}	5.79×10^{19}	3.20×10^{18}	1.42×10^{19}	7.14×10^{19}	1.34×10^{19}	$5.3^{+1.2}_{-0.8} \times 10^{19}$
$^{76}\mathrm{Ge} \to {}^{76}\mathrm{Se}$	1.42×10^{22}	5.85×10^{21}	2.97×10^{20}	2.82×10^{22}	1.98×10^{22}	3.05×10^{21}	$(1.88 \pm 0.08) \times 10^{21}$
$^{82}\mathrm{Se} \to {}^{82}\mathrm{Kr}$	4.34×10^{20}	6.97×10^{19}	9.59×10^{18}	9.95×10^{20}	2.92×10^{20}	1.19×10^{20}	$\left(0.87^{+0.02}_{-0.01}\right) \times 10^{20}$
$^{96}\mathrm{Zr} \to {}^{96}\mathrm{Mo}$	7.50×10^{18}	1.86×10^{18}	2.23×10^{18}	2.40×10^{19}	1.29×10^{19}	4.35×10^{19}	$(2.3 \pm 0.2) \times 10^{19}$
$^{100}\mathrm{Mo} \to {}^{100}\mathrm{Ru}$	5.32×10^{17}	5.00×10^{17}	3.53×10^{17}	1.88×10^{18}	4.01×10^{18}	7.82×10^{18}	$\left(7.06^{+0.15}_{-0.13}\right) \times 10^{18}$
$^{116}\mathrm{Cd} \to {}^{116}\mathrm{Sn}$	2.77×10^{18}	1.85×10^{18}	1.23×10^{18}	1.44×10^{19}	2.64×10^{19}	4.53×10^{19}	$(2.69 \pm 0.09) \times 10^{19}$
$^{128}\mathrm{Te} \to {}^{128}\mathrm{Xe}$	9.28×10^{23}	1.31×10^{23}	1.48×10^{23}	6.41×10^{24}	2.87×10^{24}	8.03×10^{24}	$(2.25 \pm 0.09) \times 10^{24}$
$^{130}\mathrm{Te} \to {}^{130}\mathrm{Xe}$	1.67×10^{21}	9.48×10^{19}	9.29×10^{18}	1.21×10^{22}	2.24×10^{21}	5.37×10^{20}	$(7.91 \pm 0.21) \times 10^{20}$
$^{136}\mathrm{Xe} \to {}^{136}\mathrm{Ba}$	3.49×10^{19}	1.86×10^{19}	3.13×10^{18}	2.93×10^{20}	5.44×10^{20}	2.20×10^{20}	$(2.18 \pm 0.05) \times 10^{21}$
$^{150}\mathrm{Nd} \to {}^{150}\mathrm{Sm}$	1.18×10^{17}	7.78×10^{16}	4.21×10^{16}	1.39×10^{18}	3.77×10^{18}	4.61×10^{18}	$(9.34 \pm 0.65) \times 10^{18}$
$^{100}\mathrm{Mo} \to {}^{100}\mathrm{Ru}(0_2^+)$	8.78×10^{19}	2.68×10^{20}	2.22×10^{21}	3.10×10^{20}	2.15×10^{21}	4.91×10^{22}	$6.7^{+0.5}_{-0.4} \times 10^{20}$
$^{150}\mathrm{Nd} \to {}^{150}\mathrm{Sm}(0_2^+)$	9.84×10^{18}	2.08×10^{18}	3.66×10^{18}	1.15×10^{20}	1.01×10^{20}	4.01×10^{20}	$1.2^{+0.3}_{-0.2} \times 10^{20}$

TABLE VI. Strength parameters for the boson-fermion interaction $\hat{V}_{\mathrm{BF}}^{\nu}$ (9) for the odd-odd nuclei obtained for the single-particle spaces corresponding to the positive- and negative-parity states in the cases of the reduced ($0.9V$), default (V), and increased ($1.15V$) pairing strengths in the RHB-SCMF calculations. Note that the single-neutron space for ^{48}Sc does not include orbitals of positive parity, so the strength parameters corresponding to positive parity are taken to be the same as those determined for the negative-parity ($2p_{1/2,3/2}, 1f_{5/2,7/2}$) configuration.

| | | Γ_ν (MeV) | | | Λ_ν (MeV) | | | A_ν (MeV) | | |
Nucleus	Single-particle space	0.9V	V	1.15V	0.9V	V	1.15V	0.9V	V	1.15V
^{48}Sc	$2p_{1/2,3/2}, 1f_{5/2,7/2}$	0.30	0.30	0.30	1.00	1.00	1.00			
^{76}As	$1g_{9/2}$	0.30	0.30	0.60	1.20	1.00	1.00	−0.60	−0.50	−0.50
	$2p_{1/2,3/2}, 1f_{5/2}$	0.30	0.30	0.60	0.80	0.80	1.00	−0.50	−0.50	−0.40
^{82}Br	$1g_{9/2}$	0.30	0.30	0.30	2.10	2.10	1.70			
	$2p_{1/2,3/2}, 1f_{5/2}$	0.30	0.30	0.30	0.80	0.80	0.80			
^{96}Nb	$3s_{1/2}, 2d_{3/2,5/2}, 1g_{7/2}$	0.30	0.30	0.30	0.40	0.40	0.40			
	$1h_{11/2}$	0.30	0.30	0.30				−1.50	−1.50	−0.80
^{100}Tc	$3s_{1/2}, 2d_{3/2,5/2}, 1g_{7/2}$	0.30	0.30	0.30	0.35	0.35	0.35			
	$1h_{11/2}$	0.30	0.30	0.30						
^{116}In	$3s_{1/2}, 2d_{3/2,5/2}, 1g_{7/2}$	0.30	0.30	0.30	0.20	0.20	0.20	−0.15	−0.15	−0.15
	$1h_{11/2}$	0.30	0.30	0.30	0.20	0.20	0.20	−0.15	−0.15	−0.15
^{128}I	$3s_{1/2}, 2d_{3/2,5/2}, 1g_{7/2}$	0.30	0.30	0.30	6.50	6.50	6.50			
	$1h_{11/2}$	0.30	0.30	0.30	0.90	0.90	0.90	−0.20	−0.20	−0.20
^{130}I	$3s_{1/2}, 2d_{3/2,5/2}, 1g_{7/2}$	0.30	0.30	0.30	7.60	7.60	5.00			
	$1h_{11/2}$	0.30	0.30	0.30	0.90	0.90	0.90	−0.50	−0.50	−0.50
^{136}Cs	$3s_{1/2}, 2d_{3/2,5/2}, 1g_{7/2}$	0.30	0.30	0.30	0.20	0.20	0.20	−0.15	−0.15	−0.15
	$1h_{11/2}$	0.30	0.30	0.30	0.20	0.20	0.20	−0.15	−0.15	−0.15
^{150}Pm	$1i_{13/2}$	0.30	0.30	0.30	16.00	10.00	6.00		−0.80	−0.80
	$3p_{1/2,3/2}, 2f_{5/2,7/2}, 1h_{9/2}$	0.30	0.30	0.30	0.50	0.60	0.50	−0.80		−0.80

TABLE VII. Same as Table VI, but for $\hat{V}_{\text{BF}}^{\pi}$.

Nucleus	Single-particle space	Γ_π (MeV)			Λ_π (MeV)			A_π (MeV)		
		0.9V	V	1.15V	0.9V	V	1.15V	0.9V	V	1.15V
^{48}Sc	$2p_{1/2,3/2}, 1f_{5/2,7/2}$	0.30	0.30	0.30						
^{76}As	$1g_{9/2}$	1.00	1.00	1.00						
	$2p_{1/2,3/2}, 1f_{5/2}$	0.30	0.30	0.60	1.60	1.60	0.35	-0.80	-0.80	
^{82}Br	$1g_{9/2}$	2.50	2.50	2.00			1.30			
	$2p_{1/2,3/2}, 1f_{5/2}$	0.30	0.30	0.30	0.80	0.80	0.80			
^{96}Nb	$1g_{9/2}$	0.30	0.30	0.30	0.90	0.90	0.90	-0.50	-0.50	
	$2p_{1/2,3/2}, 1f_{5/2}$	0.30	0.30	0.30	1.60	1.60	1.60	-0.30	-0.30	-0.30
^{100}Tc	$1g_{9/2}$	0.30	0.30	0.30	0.90	0.90	0.60			
	$2p_{1/2,3/2}, 1f_{5/2}$	0.30	0.30	0.30	5.00	5.00	5.00	-1.00	-1.00	-1.00
^{116}In	$1g_{9/2}$	0.30	0.30	0.30						
	$2p_{1/2,3/2}, 1f_{5/2}$	1.00	1.00	1.00						
^{128}I	$3s_{1/2}, 2d_{3/2,5/2}, 1g_{7/2}$	0.30	0.30	0.30	0.60	0.60	0.60	-1.00	-1.00	-1.00
	$1h_{11/2}$	0.30	0.30	0.30				-1.05	-1.05	-1.05
^{130}I	$3s_{1/2}, 2d_{3/2,5/2}, 1g_{7/2}$	0.30	0.30	0.30	0.80	0.80	0.80	-0.75	-0.75	-0.50
	$1h_{11/2}$	0.30	0.30	0.30				-1.05	-1.05	-1.05
^{136}Cs	$3s_{1/2}, 2d_{3/2,5/2}, 1g_{7/2}$	0.30	0.30	0.30						
	$1h_{11/2}$	1.00	1.00	1.00						
^{150}Pm	$3s_{1/2}, 2d_{3/2,5/2}, 1g_{7/2}$	0.30	0.30	0.30	0.40	0.40	0.40	-0.70	-1.00	-0.70
	$1h_{9/2,11/2}$	1.00	1.00	1.00	2.80	3.00	2.80			

for the ^{150}Nd decay,

$$\frac{\tau_{1/2}^{(2\nu)}[^{150}\text{Nd}(0_1^+) \to {}^{150}\text{Sm}(0_2^+)]}{\tau_{1/2}^{(2\nu)}[^{150}\text{Nd}(0_1^+) \to {}^{150}\text{Sm}(0_1^+)]} = 12.8_{-2.3}^{+3.3}, \qquad (30)$$

is reproduced reasonably well by the present calculation, with the predicted values being 83, 27, and 87, for the pairing strengths of $0.9V$, V, and $1.15V$, respectively. These ratios are independent of the effective g_A factors if the same g_A^{eff} values are used in the calculations of the NMEs for the $0_1^+ \to 0_1^+$ and $0_1^+ \to 0_2^+$ decays. The description of the ratio for the ^{100}Mo decays (29) could be improved if different g_A^{eff} values are considered between the $0_1^+ \to 0_1^+$ and $0_1^+ \to 0_2^+$ decays.

V. CONCLUDING REMARKS

The low-energy nuclear structure and $2\nu\beta\beta$-decay NMEs without the closure approximation have been investigated within the mapped IBM-2 that is based on the SCMF calculation employing the relativistic EDF DD-PC1 and separable pairing force of finite range. The IBM-2 Hamiltonian describing the initial and final even-even nuclei has been completely determined by mapping the RHB-SCMF PES onto the bosonic counterpart. The particle-boson and particle-particle interactions in the IBFFM-2 Hamiltonian used to compute intermediate states of the neighboring odd-odd nuclei have also been determined by using the results of the RHB-SCMF calculations. In the present analysis, the effects of changing the pairing strength in the RHB calculations on the spectroscopic properties of low-lying states and $2\nu\beta\beta$-decay NMEs have been specifically studied.

When the increased pairing with respect to the default one by 15% is chosen, the SCMF PESs for the candidate even-even nuclei have been shown to be substantially softer in both the axial β and triaxial γ deformations, and the potential valley becomes less pronounced. With the pairing strength reduced by 10% from the default one, on the other hand, a PES with a much more pronounced potential valley has been obtained which is steep in the β and γ directions. The derived strength parameters for the pairing-like term ($\hat{n}_d$) and quadrupole-quadrupole interaction ($\hat{Q}_\nu \cdot \hat{Q}_\pi$) in the IBM-2 have been shown to be significantly at variance with the different IBM-2 calculations using the reduced, default, and increased pairing strengths in the RHB-SCMF calculations.

The calculated energy spectra for the even-even nuclei indicated that with the increased pairing strength $1.15V$, the energy levels for the non-yrast states 0_2^+ and 2_2^+ are generally lowered, being in better agreement with experiment than in the cases of the weaker pairing strength $0.9V$ and V. An even more accurate description of the excited 0_2^+ states in the even-even nuclei and its influence on the $\beta\beta$-decay NMEs would be better investigated within the version of the IBM-2 that incorporates the configuration mixing between the normal and intruder states. The energy levels for the intermediate odd-odd nuclei have been shown to be more or less sensitive to the choice of the pairing strength. The electromagnetic transition properties for both the even-even and odd-odd nuclear systems have exhibited certain sensitivities to the pairing strengths. A notable consequence is that the calculation with the default pairing strength has given the best agreement with the experimental transition properties for many of the odd-odd nuclei.

TABLE VIII. Strength parameters used for the residual neutron-proton interaction $\hat{V}_{\nu\pi}$ (13) in the IBFFM-2 Hamiltonian for the intermediate odd-odd nuclei for the calculations with the three different pairing strengths. Note that the spin-spin interaction strength $v_{ss} = 0$ MeV for all the nuclei.

Nucleus	Pairing	v_d (MeV)	v_{ssd} (MeV)	v_t (MeV)
^{48}Sc	0.9V	0.60		
	V	0.60		
	1.15V	0.60		−0.02
^{76}As	0.9V	0.80		0.15
	V	0.80		0.15
	1.15V	0.80		0.02
^{82}Br	0.9V		−0.23	0.10
	V		−0.23	0.10
	1.15V		−0.23	0.10
^{96}Nb	0.9V	0.80	0.25	
	V	0.80		
	1.15V	0.40	0.10	
^{100}Tc	0.9V	−0.08		0.12
	V	−0.08		0.05
	1.15V	−0.08		0.20
^{116}In	0.9V	−0.80		0.40
	V	−0.80		0.40
	1.15V	−0.80		0.43
^{128}I	0.9V		−0.05	
	V		−0.51	
	1.15V		−0.30	
^{130}I	0.9V	−0.02		0.01
	V	−0.08		0.01
	1.15V	0.01		0.01
^{136}Cs	0.9V	−0.08		0.15
	V	−0.08		0.09
	1.15V	−0.08		0.04
^{150}Pm	0.9V	−0.08		0.20
	V	−0.08		0.14
	1.15V	−0.08		0.18

An effect of modifying the pairing strength in the RHB-SCMF calculation on $2\nu\beta\beta$ decay is that with the increased strength, resultant $2\nu\beta\beta$-decay NMEs, $|M_{2\nu}|$, become systematically larger. A quenching of the NMEs with the effective g_A^{eff} factor that is a smooth function of the mass A has been introduced as in Ref. [27]. In the calculation employing the increased pairing strength $1.15V$, the effective NMEs turned out be in a fairly good agreement with the experimental $|M_{2\nu}^{eff}|$ values for the ^{76}Ge, ^{82}Se, and ^{100}Mo decays in particular. In many other decays, however, the calculated results with the default V pairing strength have been shown to be adequate to provide an overall good agreement with the data.

Of several assumptions, and approximations introduced in the employed theoretical approach, the uncertainties in the $2\nu\beta\beta$ NME predictions could arise, to a larger extent, from the SCMF models and properties of the employed EDF, which underlie the mapped IBM-2 study. The present study indicates that the strength of the pairing interaction is considered among the most important parameters that may affect both low-lying states and decay processes. In the meantime, it remains an open question to investigate thoroughly how relevant other building blocks involved in the model are in the predictions of the NMEs, as well as the low-lying structures, such as those related to the parametrizations of the EDF, to the single-particle properties, to other missing correlations at the SCMF level, and to the forms of the IBM-2 and IBFFM-2 Hamiltonians.

APPENDIX: PARAMETERS FOR THE IBFFM-2 HAMILTONIAN

The strength parameters adopted for the boson-fermion interactions $\hat{V}_{BF}^{\nu}$ and $\hat{V}_{BF}^{\pi}$, and the residual neutron-proton interaction $\hat{V}_{\nu\pi}$ in the IBFFM-2 Hamiltonian in the three cases of the separable pairing strength in the RHB-SCMF calculations are listed in Tables VI, VII, and VIII, respectively. Some updates have been made to the adopted IBFFM-2 parameters since the previous study of Ref. [27] concerning the parameters Λ_ν, A_ν, for both parities, and the tensor strength v_t, for the nucleus ^{76}As, when the default pairing strength V is used. New parameters are here also employed for some other nuclei: v_t for ^{82}Br, boson-fermion interactions for ^{136}Cs and ^{150}Pm. For details, compare entries in Tables VI, VII, and VII, with those in Table XVI of Ref. [27].

[1] H. Primakoff and S. P. Rosen, Rep. Prog. Phys. **22**, 121 (1959).

[2] W. C. Haxton, Jr. and G. Stephenson, Prog. Part. Nucl. Phys. **12**, 409 (1984).

[3] M. Doi, T. Kotani, and E. Takasugi, Prog. Theor. Phys. Suppl. **83**, 1 (1985).

[4] T. Tomoda, Rep. Prog. Phys. **54**, 53 (1991).

[5] J. Suhonen and O. Civitarese, Phys. Rep. **300**, 123 (1998).

[6] A. Faessler and F. Simkovic, J. Phys. G: Nucl. Part. Phys. **24**, 2139 (1998).

[7] P. Vogel, J. Phys. G: Nucl. Part. Phys. **39**, 124002 (2012).

[8] J. D. Vergados, H. Ejiri, and F. Šimkovic, Rep. Prog. Phys. **75**, 106301 (2012).

[9] J. Engel and J. Menéndez, Rep. Prog. Phys. **80**, 046301 (2017).

[10] F. T. Avignone, S. R. Elliott, and J. Engel, Rev. Mod. Phys. **80**, 481 (2008).

[11] H. Ejiri, J. Suhonen, and K. Zuber, Phys. Rep. **797**, 1 (2019).

[12] M. Agostini, G. Benato, J. A. Detwiler, J. Menéndez, and F. Vissani, Rev. Mod. Phys. **95**, 025002 (2023).

[13] A. Barabash, Universe **6**, 159 (2020).

[14] M. Agostini, A. Alexander, G. R. Araujo, A. M. Bakalyarov, M. Balata, I. Barabanov, L. Baudis, C. Bauer, S. Belogurov, A. Bettini, L. Bezrukov, V. Biancacci, E. Bossio, V. Bothe, R. Brugnera, A. Caldwell, S. Calgaro, C. Cattadori,

A. Chernogorov, P.-J. Chiu (GERDA Collaboration) *et al.*, Phys. Rev. Lett. **131**, 142501 (2023).

[15] C. Augier, A. S. Barabash, F. Bellini, G. Benato, M. Beretta, L. Bergé, J. Billard, Y. A. Borovlev, L. Cardani, N. Casali, A. Cazes, E. Celi, M. Chapellier, D. Chiesa, I. Dafinei, F. A. Danevich, M. De Jesus, T. Dixon, L. Dumoulin, K. Eitel (CUPID-Mo Collaboration) *et al.*, Phys. Rev. Lett. **131**, 162501 (2023).

[16] C. Augier, A. S. Barabash, F. Bellini, G. Benato, M. Beretta, L. Bergé, J. Billard, Y. A. Borovlev, L. Cardani, N. Casali, A. Cazes, M. Chapellier, D. Chiesa, I. Dafinei, F. A. Danevich, M. De Jesus, T. Dixon, L. Dumoulin, K. Eitel, F. Ferri (CUPID-Mo Collaboration) *et al.*, Phys. Rev. C **107**, 025503 (2023).

[17] D. Q. Adams, C. Alduino, K. Alfonso, F. T. Avignone, O. Azzolini, G. Bari, F. Bellini, G. Benato, M. Biassoni, A. Branca, C. Brofferio, C. Bucci, J. Camilleri, A. Caminata, A. Campani, L. Canonica, X. G. Cao, S. Capelli, L. Cappelli *et al.*, Phys. Rev. Lett. **126**, 171801 (2021).

[18] P. Pirinen and J. Suhonen, Phys. Rev. C **91**, 054309 (2015).

[19] F. Šimkovic, A. Smetana, and P. Vogel, Phys. Rev. C **98**, 064325 (2018).

[20] E. Caurier, F. Nowacki, and A. Poves, Int. J. Mod. Phys. E **16**, 552 (2007).

[21] N. Yoshinaga, K. Yanase, K. Higashiyama, E. Teruya, and D. Taguchi, Prog. Theor. Exp. Phys. **2018**, 023D02 (2018).

[22] E. Caurier, A. Poves, and A. Zuker, Phys. Lett. B **252**, 13 (1990).

[23] E. Caurier, F. Nowacki, and A. Poves, Phys. Lett. B **711**, 62 (2012).

[24] R. A. Sen'kov and M. Horoi, Phys. Rev. C **93**, 044334 (2016).

[25] L. Coraggio, L. De Angelis, T. Fukui, A. Gargano, N. Itaco, and F. Nowacki, Phys. Rev. C **100**, 014316 (2019).

[26] N. Yoshida and F. Iachello, Prog. Theor. Exp. Phys. **2013**, 043D01 (2013).

[27] K. Nomura, Phys. Rev. C **105**, 044301 (2022).

[28] T. Otsuka, A. Arima, F. Iachello, and I. Talmi, Phys. Lett. B **76**, 139 (1978).

[29] T. Otsuka, A. Arima, and F. Iachello, Nucl. Phys. A **309**, 1 (1978).

[30] P. Ring and P. Schuck, *The Nuclear Many-Body Problem* (Springer, Berlin, 1980).

[31] M. Bender, P.-H. Heenen, and P.-G. Reinhard, Rev. Mod. Phys. **75**, 121 (2003).

[32] D. Vretenar, A. V. Afanasjev, G. A. Lalazissis, and P. Ring, Phys. Rep. **409**, 101 (2005).

[33] T. Nikšić, D. Vretenar, and P. Ring, Prog. Part. Nucl. Phys. **66**, 519 (2011).

[34] L. M. Robledo, T. R. Rodríguez, and R. R. Rodríguez-Guzmán, J. Phys. G: Nucl. Part. Phys. **46**, 013001 (2019).

[35] T. Nikšić, D. Vretenar, and P. Ring, Phys. Rev. C **78**, 034318 (2008).

[36] Y. Tian, Z. Y. Ma, and P. Ring, Phys. Lett. B **676**, 44 (2009).

[37] S. Brant, V. Paar, and D. Vretenar, Z. Phys. A **319**, 355 (1984).

[38] F. Iachello and P. Van Isacker, *The Interacting Boson-Fermion Model* (Cambridge University Press, Cambridge, 1991).

[39] P. D. Duval and B. R. Barrett, Phys. Lett. B **100**, 223 (1981).

[40] K. Nomura, T. Otsuka, and P. Van Isacker, J. Phys. G: Nucl. Part. Phys. **43**, 024008 (2016).

[41] K. Nomura, R. Rodríguez-Guzmán, and L. M. Robledo, Phys. Rev. C **94**, 044314 (2016).

[42] K. Nomura, Phys. Rev. C **106**, 024330 (2022).

[43] K. Nomura, D. Vretenar, Z. P. Li, and J. Xiang, Phys. Rev. C **102**, 054313 (2020).

[44] K. Nomura, D. Vretenar, Z. P. Li, and J. Xiang, Phys. Rev. C **103**, 054322 (2021).

[45] K. Nomura, N. Gavrielov, and A. Leviatan, Phys. Rev. C **104**, 044317 (2021).

[46] M. Homma and K. Nomura, Phys. Rev. C **110**, 014303 (2024).

[47] J. F. Berger, M. Girod, and D. Gogny, Nucl. Phys. A **428**, 23 (1984).

[48] S. Teeti and A. V. Afanasjev, Phys. Rev. C **103**, 034310 (2021).

[49] A. Bohr and B. R. Mottelson, *Nuclear Structure* (Benjamin, New York, 1975).

[50] K. Nomura, T. Nikšić, and D. Vretenar, Phys. Rev. C **93**, 054305 (2016).

[51] K. Nomura, R. Rodríguez-Guzmán, and L. M. Robledo, Phys. Rev. C **96**, 014314 (2017).

[52] K. Nomura, N. Shimizu, and T. Otsuka, Phys. Rev. Lett. **101**, 142501 (2008).

[53] K. Nomura, N. Shimizu, and T. Otsuka, Phys. Rev. C **81**, 044307 (2010).

[54] A. E. L. Dieperink, O. Scholten, and F. Iachello, Phys. Rev. Lett. **44**, 1747 (1980).

[55] J. N. Ginocchio and M. W. Kirson, Nucl. Phys. A **350**, 31 (1980).

[56] K. Nomura, T. Otsuka, N. Shimizu, and L. Guo, Phys. Rev. C **83**, 041302(R) (2011).

[57] H. Schaaser and D. M. Brink, Nucl. Phys. A **452**, 1 (1986).

[58] D. R. Inglis, Phys. Rev. **103**, 1786 (1956).

[59] S. T. Beliaev, Nucl. Phys. **24**, 322 (1961).

[60] O. Scholten, Prog. Part. Nucl. Phys. **14**, 189 (1985).

[61] K. Nomura, R. Rodríguez-Guzmán, and L. M. Robledo, Phys. Rev. C **99**, 034308 (2019).

[62] F. Dellagiacoma, Beta decay of odd mass nuclei in the interacting boson-fermion model, Ph.D. thesis, Yale University, 1988.

[63] F. Dellagiacoma and F. Iachello, Phys. Lett. B **218**, 399 (1989).

[64] Brookhaven National Nuclear Data Center, http://www.nndc.bnl.gov.

[65] J. Kotila and F. Iachello, Phys. Rev. C **85**, 034316 (2012).

[66] N. Stone, At. Data Nucl. Data Tables **90**, 75 (2005).

[67] J. Barea, J. Kotila, and F. Iachello, Phys. Rev. C **87**, 014315 (2013).

[68] J. Barea, J. Kotila, and F. Iachello, Phys. Rev. C **91**, 034304 (2015).

[69] A. Griffiths and P. Vogel, Phys. Rev. C **46**, 181 (1992).

[70] O. Civitarese and J. Suhonen, Phys. Rev. C **58**, 1535 (1998).

[71] O. Moreno, R. Álvarez-Rodríguez, P. Sarriguren, E. M. de Guerra, F. Šimkovic, and A. Faessler, J. Phys. G: Nucl. Part. Phys. **36**, 015106 (2009).